Monthly Notices
of the
ROYAL ASTRONOMICAL SOCIETY

MNRAS **473,** 5476–5491 (2018)
Advance Access publication 2017 October 25

doi:10.1093/mnras/stx2771

Two-component Jaffe models with a central black hole – I. The spherical case

Luca Ciotti★ and Azadeh Ziaee Lorzad★

Department of Physics and Astronomy, University of Bologna, via Gobetti 93/3, I-40129 Bologna, Italy

Accepted 2017 October 23. Received 2017 October 23; in original form 2017 July 21

ABSTRACT

Dynamical properties of spherically symmetric galaxy models where both the stellar and total mass density distributions are described by the Jaffe (1983) profile (with different scalelengths and masses) are presented. The orbital structure of the stellar component is described by Osipkov–Merritt anisotropy, and a black hole (BH) is added at the centre of the galaxy; the dark matter halo is isotropic. First, the conditions required to have a nowhere negative and monotonically decreasing dark matter halo density profile are derived. We then show that the phase-space distribution function can be recovered by using the Lambert–Euler W function, while in absence of the central BH only elementary functions appears in the integrand of the inversion formula. The minimum value of the anisotropy radius for consistency is derived in terms of the galaxy parameters. The Jeans equations for the stellar component are solved analytically, and the projected velocity dispersion at the centre and at large radii are also obtained analytically for generic values of the anisotropy radius. Finally, the relevant global quantities entering the Virial Theorem are computed analytically, and the fiducial anisotropy limit required to prevent the onset of Radial Orbit Instability is determined as a function of the galaxy parameters. The presented models, even though highly idealized, represent a substantial generalization of the models presented in Ciotti, and can be useful as starting point for more advanced modelling, the dynamics and the mass distribution of elliptical galaxies.

Key words: celestial mechanics – galaxies: elliptical and lenticular, cD – galaxies: kinematics and dynamics.

1 INTRODUCTION

Spherically symmetric galaxy models, despite their simplicity, are useful tools for theoretical and observational works in Stellar Dynamics, and for the modellization of stellar systems (e.g. Bertin 2000; Binney & Tremaine 2008). Quite obviously spherical symmetry is an oversimplification when considering the vast majority of stellar systems, and a useful spherical model must compensate this limitation with other features, which make its use preferred or even recommended, especially in preliminary investigations. Among the important features of a useful spherical model here, we list analytical simplicity, structural and dynamical flexibility, i.e. possibility to add to the stellar component a dark matter (DM) halo with adjustable density profile, or alternatively to specify the total density profile, to include the dynamical effects of a central black hole (BH), to control orbital anisotropy

For example, the density profile of the stellar distribution of the model, once projected, should be similar to that of early-type galaxies, i.e. to the de Vaucouleurs (1948) $R^{1/4}$ law, or better, to its generalization, the so-called $R^{1/m}$ law (Sersic 1963). Unfortunately, the $R^{1/m}$ law does not allow for an explicit deprojection in terms of elementary functions; however, the so-called γ models (Dehnen 1993; Tremaine et al. 1994) in projection are well fitted over a large radial range, by the $R^{1/m}$ law. This is especially true for the Jaffe (1983) and Hernquist (1990) models.

Another important feature of a useful spherical model is the possibility to reproduce the large-scale observational properties of the *total* density profile of early-type galaxies. In fact, analysis of stellar kinematics (e.g. Bertin, Ciotti & Del Principe 1994a; Rix et al. 1997; Gerhard et al. 2001), as well as several studies combining stellar dynamics and gravitational lensing, supports the idea that the dark and the stellar matter in elliptical galaxies are distributed so that their total mass profile is described by a density distribution proportional to r^{-2} (e.g. see Treu & Koopmans 2002, 2004; Rusin, Kochanek & Keeton 2003; Rusin & Kochanek 2005; Koopmans et al. 2006; Gavazzi et al. 2007; Czoske et al. 2008; Dye et al. 2008; Nipoti, Treu & Bolton 2008; Shankar et al. 2017). It is clear that simple dynamical models of two-component galaxies can be useful as starting point of more sophisticated investigations based on axisymmetric or triaxial galaxy models (e.g. Cappellari et al. 2007;

★ E-mail: luca.ciotti@unibo.it (LC); azadeh.ziaeelorzad@studio.unibo.it (AZL)

van den Bosch et al. 2008). Simple models with flat rotation curve have been in fact constructed (e.g. Kochanek 1994; Naab & Ostriker 2007). In particular, we recall the family of two-component galaxy models whose total mass density is proportional to r^{-2}, while the visible (stellar) mass is described by the γ models (Ciotti, Morganti & de Zeeuw 2009, hereafter CMZ09; see also the double power-law models of Hiotelis 1994). These latter models have been used in hydrodynamical simulations of accretion on to the central supermassive BH in elliptical galaxies (Ciotti & Ostriker 2012, and references therein). We notice that other models built with the same approach have been recently applied for the interpretation of observations (Poci, Cappellari & McDermid 2017). We also remark that the approach used to build these models is different from the standard one, where a DM halo is *added* to the stellar distribution (e.g. Ciotti & Renzini 1993; Ciotti, Lanzoni & Renzini 1996, hereafter CRL96; Ciotti 1996, 1999; section 4.4 in CMZ09).

A third important feature of a useful spherical model, strictly related to the previous point, is the possibility to easily compute the dynamical properties of the stellar component in presence of a central BH, and possibly to be proved dynamically consistent (see Section 3.1). In fact, supermassive BHs with a mass of the order of $M_{\rm BH} \simeq 10^{-3} M_*$ are routinely found at the centre of the stellar spheroids of total mass M_* (e.g. see Magorrian et al. 1998; Kormendy & Ho 2013).

Following the arguments above, this paper builds on the CMZ09 model, and present an even more general (and realistic) class of models, containing the CMZ09 model as a limit case. On one side, we maintain the assumption of a Jaffe profile for the stellar distribution, but now the total density profile is described by another Jaffe law (instead of a pure r^{-2} law), so that the total mass of the models (that we call JJ models) is finite. At the same time, the scalelength of the total density is a free parameter and so we can reproduce an r^{-2} profile over an arbitrary large radial range. Finally, a central BH of arbitrary mass (missing in CMZ09 models) is considered when solving the dynamical equations. For JJ models, we show that the Jeans equations for the stellar component with Osipkov–Merritt (OM; Osipkov 1979; Merritt 1985a) radial anisotropy can be solved analytically, and the projected velocity dispersion at the centre and at large radii can be expressed by means of extremely simple formulae for generic values of the model parameters. The positivity of the phase-space density distribution function (DF) of the stellar component, the so-called consistency, is easily investigated by using a remarkable property of JJ models, i.e. the fact that the radial coordinate can be written in terms of the total potential in terms of the so-called Lambert–Euler W function. By using this property, we determine the maximum amount of radial anisotropy allowable for consistency as a function of the galaxy parameters. These results add to the large amount of phase-space information already available about one- and two-component γ models (e.g. Carollo, de Zeeuw & van der Marel 1995; Ciotti 1996, 1999; Baes, Dejonghe & Buyle 2005; Buyle, Hunter & Dejonghe 2007; Ciotti & Morganti 2009). As a by-product of our analysis, we also found that the one-component Jaffe model, at variance with statements in the literature, *cannot* be supported by purely radial orbits. We note that the W function also appears in the recently discovered analytical solution of the isothermal Bondi accretion problem in Jaffe galaxies with central BH (Ciotti & Pellegrini 2017), and this fact suggests a first natural application of JJ models outside the field of Stellar Dynamics, namely in the field of BH accretion and active galactic nucleus (AGN) feedback.

The paper is organized as follows. In Section 2, the main structural properties of the models are presented. In Section 3, an investigation of the phase-space properties of the models is carried out both from the point of view of necessary and sufficient conditions for consistency and from direct inspection of the DF. In Section 4, the solution of the Jeans equation with OM radial anisotropy is presented, together with the projection of the velocity dispersion profile at small and large radii. In Section 5, the important properties related to the Virial Theorem (VT) and global energetic are explicitly calculated, and the maximum amount of radial anisotropy that can be sustained by the model without developing Radial Orbit Instability (ROI) is estimated. The main results are summarized in Section 6, while more technical details are given in the Appendix.

2 THE MODELS

As anticipated in the Introduction section, the present models are characterized by a *total* density distribution (stars plus DM) $\rho_{\rm g}$ described by a Jaffe (1983) profile; the stellar density distribution ρ_* is also described by a Jaffe profile, in general, with a different scale radius. For future use we recall that the Jaffe density of total mass $M_{\rm J}$ and scalelength $r_{\rm J}$ is given by

$$\rho_{\rm J}(r) = \frac{M_{\rm J} r_{\rm J}}{4\pi r^2 (r_{\rm J}+r)^2}. \tag{1}$$

The cumulative mass contained within the sphere of radius r, and the associated gravitational potential (with the natural condition of vanishing at infinity, pertinent to systems of finite mass), are given by

$$M_{\rm J}(r) = \frac{M_{\rm J} r}{r_{\rm J}+r}, \quad \Phi_{\rm J}(r) = \frac{G M_{\rm J}}{r_{\rm J}} \ln \frac{r}{r_{\rm J}+r}. \tag{2}$$

Moreover the Jaffe model belongs to the family of γ-models

$$\rho_\gamma(r) = \frac{(3-\gamma) M_\gamma r_\gamma}{4\pi r^\gamma (r_\gamma + r)^{4-\gamma}}, \quad 0 \le \gamma < 3, \tag{3}$$

where M_γ is the total mass, r_γ is a scalelength and equation (1) is obtained for $\gamma = 2$. The cumulative mass within the sphere of radius r is given by

$$M_\gamma(r) = M_\gamma \times \left(\frac{r}{r_\gamma + r}\right)^{3-\gamma}, \tag{4}$$

so that the half-mass (spatial) radius is $r_{\rm h} = r_\gamma/(2^{\frac{1}{3-\gamma}} - 1)$, and $r_{\rm h} = r_{\rm J}$ for the Jaffe model. For generic values of γ the projected density at radius R in the projection plane is given by

$$\Sigma_\gamma(R) = 2\int_R^\infty \frac{\rho_\gamma(r) r \,{\rm d}r}{\sqrt{r^2 - R^2}} \tag{5}$$

(e.g. Binney & Tremaine 2008), but unfortunately it cannot be expressed in terms of elementary functions. However, for $\gamma = 2$

$$\Sigma_{\rm J}(R) = \frac{M_{\rm J}}{r_{\rm J}^2} \times \begin{cases} \dfrac{1}{4\eta} + \dfrac{\sqrt{1-\eta^2} - (2-\eta^2)\,{\rm arcsech}(\eta)}{2\pi(1-\eta^2)^{3/2}}, & 0 < \eta < 1; \\ \dfrac{1}{4} - \dfrac{2}{3\pi}, & \eta = 1; \\ \dfrac{1}{4\eta} - \dfrac{\sqrt{\eta^2-1} + (\eta^2-2)\,{\rm arcsec}(\eta)}{2\pi(\eta^2-1)^{3/2}}, & \eta > 1; \end{cases} \tag{6}$$

where $\eta \equiv R/r_{\rm J}$. In the central and in the very external regions, the projected density profile behave like a power law, with

$$\Sigma_{\rm J}(R) \sim \frac{M_{\rm J}}{r_{\rm J}^2} \times \begin{cases} \dfrac{1}{4\eta}, & R \to 0; \\ \dfrac{1}{8\eta^3}, & R \to \infty; \end{cases} \tag{7}$$

respectively. Finally, an important structural property that we will consider in the following is the projected mass $M_{\rm p}(R)$ contained within the cylinder of radius R. It can be proved that for spherical systems of finite total mass

$$M_{\rm p}(R) \equiv 2\pi \int_0^R \Sigma(R)\, R\, {\rm d}R = M - 4\pi \int_R^\infty \rho(r) r \sqrt{r^2 - R^2} {\rm d}r. \tag{8}$$

It follows that the projected mass of the Jaffe model is given by $M_{\rm pJ}(R) = M_{\rm J} \times g(\eta)$, where

$$g(\eta) = \eta \times \begin{cases} \dfrac{\pi}{2} - \dfrac{\eta\, {\rm arcsech}(\eta)}{\sqrt{1-\eta^2}}, & 0 < \eta < 1; \\ \dfrac{\pi}{2} - 1, & \eta = 1; \\ \dfrac{\pi}{2} - \dfrac{\eta\, {\rm arcsec}(\eta)}{\sqrt{\eta^2-1}}, & \eta > 1. \end{cases} \tag{9}$$

In particular, the effective radius $R_{\rm e}$ of the Jaffe profile (i.e. the radius in the projection plane encircling half of the total mass), where $g(\eta_{\rm e}) = 1/2$, is $R_{\rm e} \simeq 0.7447 r_{\rm J}$ (in the Jaffe original paper the slightly erroneous value of 0.763 is reported).

2.1 Stellar and total mass distribution

We denote our family of models as 'JJ' models, to indicate that it is a two-component Jaffe model, even though constructed in a different way with respect to other two-components Jaffe models in the literature (CLR96; Ciotti 1996, 1999). The properties of the stellar component are obtained with $M_{\rm J} = M_*$ and $r_{\rm J} = r_*$ in equations (1)–(9), while for the galaxy total density distribution (stars plus DM) $M_{\rm J} = M_{\rm g}$ and $r_{\rm J} = r_{\rm g}$. We adopt M_* and r_* as the natural mass and length scales, and we define

$$s \equiv \frac{r}{r_*}, \quad \xi \equiv \frac{r_{\rm g}}{r_*}, \quad \mathcal{R} \equiv \frac{M_{\rm g}}{M_*} = \mathcal{R}_{\rm DM} + 1. \tag{10}$$

From the request that the DM component has a non-negative total mass $M_{\rm DM}$ it follows that $\mathcal{R}_{\rm DM} \equiv M_{\rm DM}/M_* \geq 0$, and so $\mathcal{R} \geq 1$. It is important to note that the request of a non-negative $M_{\rm DM}$ does not prevent the possibility of an unphysical, *locally negative* DM density. This case will be excluded with the introduction of an additional constraint, determined in Section 2.2. We also define

$$\rho_{\rm n} \equiv \frac{M_*}{4\pi r_*^3}, \quad \Psi_{\rm n} \equiv \frac{GM_*}{r_*}, \tag{11}$$

as the natural density and potential scales. With these conventions, equations (1) and (2) for the galaxy model become

$$\rho_{\rm g}(r) = \frac{\mathcal{R}\xi\rho_{\rm n}}{s^2(\xi+s)^2}, \tag{12}$$

and

$$M_{\rm g}(r) = \frac{M_*\mathcal{R}s}{\xi+s}, \quad \Phi_{\rm g}(r) = \frac{\mathcal{R}\Psi_{\rm n}}{\xi} \ln\frac{s}{\xi+s}. \tag{13}$$

We note here an important connection of the JJ models with the models in CMZ09. In fact, the total galaxy density profile in CMZ09 (equation 6 therein) can be written as

$$\rho_{\rm g}^{\rm CMZ}(r) = \frac{v_0^2}{4\pi G r^2} = \frac{\mathcal{R}_{\rm CMZ}\rho_{\rm n}}{s^2}, \tag{14}$$

where v_0 is the constant circular velocity. As the total mass associated with equation (14) diverges, the parameter $\mathcal{R}_{\rm CMZ} = v_0^2/\Psi_{\rm n}$ is *not* the ratio of the total-to-stellar mass as in JJ models. An elementary integration shows that $\mathcal{R}_{\rm CMZ} = M_{\rm g}(r_*)/M_*$, i.e. it is the *total* mass contained within the half-mass radius of the Jaffe stellar density profile, normalized to the total stellar mass. From equations (12) and (14), it follows that the total density distribution (and the associated quantities, such as the cumulative and the projected mass profiles, and the force field) of CMZ09 models can be obtained from JJ models with the substitution

$$\mathcal{R} = \mathcal{R}_{\rm CMZ}\xi \tag{15}$$

in the corresponding quantities, and then considering the limit for $\xi \to \infty$. Some care is needed for the case of the potential. In fact JJ models, have finite mass and vanishing potential at infinity, while the logarithmic potential of CMZ09 models

$$\Phi_{\rm g}^{\rm CMZ}(r) = v_0^2 \ln s, \tag{16}$$

diverges for $s \to \infty$. The proper way to reobtain $\Phi_{\rm g}^{\rm CMZ}$ from equation (13) is to apply the substitution (15) to JJ scaled potential $\Phi_{\rm g} + \mathcal{R}\Psi_{\rm n}(\ln\xi)/\xi$, and then to take the limit $\xi \to \infty$.

2.2 The DM distribution: positivity and monotonicity

Before studying the dynamical properties of the models, it is important to determine the conditions for the positivity and radial monotonicity of the density distribution of the DM halo. While as anticipated in Section 2.1 the request of positivity is natural, a brief comment is in order to justify the requirement of monotonicity. In fact, it can be shown that monotonicity of the density as a function of the potential is necessary for the positivity of the phase-space DF. From the second Newton's theorem, the gravitational potential of a spherical system is necessarily radially monotone, so that the density profile must be a monotone function of radius (Ciotti & Pellegrini 1992, hereafter CP92; see also Section 3).

As already found in the simpler two-component model of CMZ09, also in JJ models, not all values of $\mathcal{R}$ and ξ are compatible with a nowhere negative DM distribution $\rho_{\rm DM}$. Curiously, it is possible to obtain analytically the positivity condition for the more general family of two-component γ models, built with the same approach of JJ models. For $\gamma\gamma$ models, the DM distribution can be written as

$$\rho_{\rm DM}(r) = \frac{(3-\gamma)\rho_{\rm n}}{s^\gamma}\left[\frac{\mathcal{R}\xi}{(\xi+s)^{4-\gamma}} - \frac{1}{(1+s)^{4-\gamma}}\right]. \tag{17}$$

Note that $\rho_{\rm DM}$ of $\gamma\gamma$ models *is not a γ model, unless the stellar and total length scale are equal*, so that, in general, the local DM-to-stellar mass ratio $\rho_{\rm DM}(r)/\rho_*(r)$ depends on r. It is easy to verify that the total DM mass associated with $\rho_{\rm DM}$ is $M_{\rm DM} = 4\pi\rho_{\rm n} r_*^3(\mathcal{R}-1)$.

In Appendix A, we determine, for given $0 \leq \gamma < 3$, the conditions on $\mathcal{R}$ and ξ to have $\rho_{\rm DM} \geq 0$ for $r \geq 0$. In the case of the JJ models (i.e. $\gamma\gamma$ models with $\gamma = 2$), the positivity condition (A2) reduces to

$$\mathcal{R} \geq \mathcal{R}_{\rm m}(\xi) = \max\left(\frac{1}{\xi}, \xi\right), \tag{18}$$

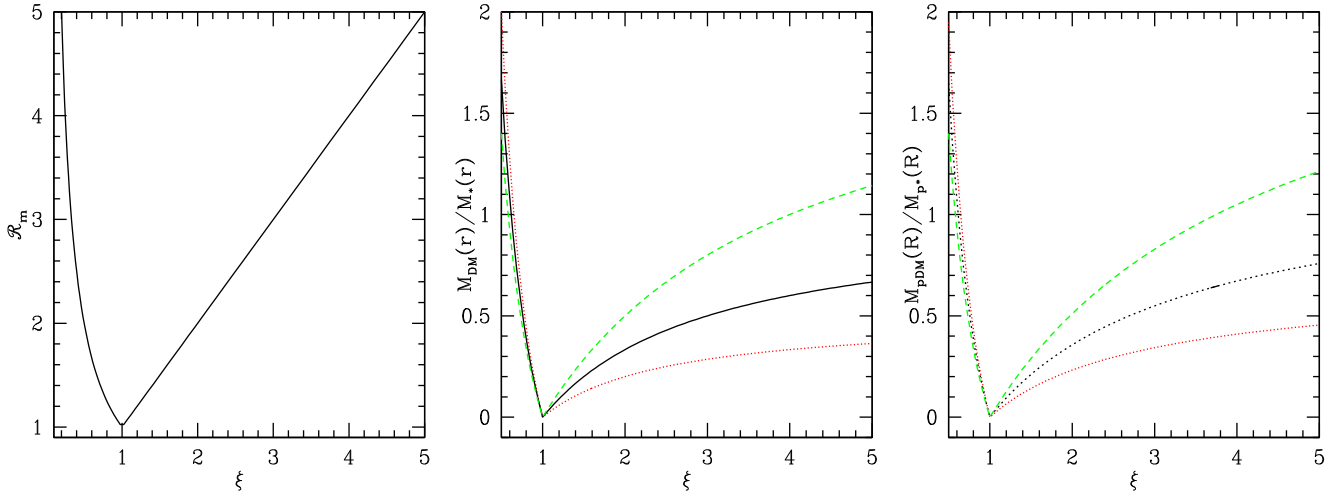

Figure 1. Left-hand panel: the minimum value of the total-to-stellar mass ratio $\mathcal{R}_m$, as a function of $\xi = r_g/r_*$, as given by equation (18). Only models in the open triangular region are characterized by a DM halo with a nowhere negative density ρ_{DM}. Central panel: the minimum value of the volumic DM-to-stellar mass ratio inside a sphere of radius $r = 0.5r_*$, r_* and $2r_*$ (red dotted, black solid and green dashed lines, respectively), as a function of ξ. Right-hand panel: the minimum value of the projected DM-to-stellar mass ratio inside the circle of radius $R = 0.5R_e$, R_e and $2R_e$ (red dotted, black solid, green dashed lines, respectively), as a function of ξ.

a DM halo of a model with $\mathcal{R} = \mathcal{R}_m$ is called a *minimum halo*. From equation above, it follows that more and more DM is needed for a total density distribution ρ_g more and more contracted, or more and more expanded than the stellar distribution ρ_*. The minimum value $\mathcal{R}_m = 1$ can be only adopted when $\xi = 1$, i.e. when the stellar and total density are proportional, and so ρ_{DM} can vanish everywhere. The situation is illustrated in Fig. 1 (left-hand panel).

As anticipated the positivity of ρ_{DM} is just a first condition for the viability of the model. A second request is the monotonicity of ρ_{DM} as a function of radius, and this reduces to the determination of the minimum value $\mathcal{R}_{mon}$ so that $d\rho_{DM}/dr \leq 0$. The explicit discussion of this additional restriction is given in Appendix A, for the whole family of $\gamma\gamma$ models. In particular, we found that for $1 \leq \gamma < 3$ (the range containing JJ models, or the analogous two-component Hernquist models), the positivity and monotonicity conditions for ρ_{DM} coincide, i.e. $\mathcal{R}_{mon}(\xi) = \mathcal{R}_m(\xi)$.

Equation (18) allows to discuss the relative trend of DM and stars in JJ models, both at large radii and near the centre, as a function of $\mathcal{R}$ and ξ. For $r \to \infty$ and $\xi > 1$, it is easy to show that $\rho_{DM} \sim (\mathcal{R}\xi - 1)\rho_*$, and so in the outskirts, DM and stars are proportional. When $\xi < 1$ instead the situation is more complicated: while in non-minimum halo models $\rho_{DM} \sim (\mathcal{R}/\xi - 1)\rho_*$ and so DM and stars distributions are again proportional, in the minimum halo case $\rho_{DM} \sim 2(1-\xi)\rho_*/s \propto r^{-5}$, so that the galaxy is baryon-dominated in the external regions. The situation inverts for $r \to 0$. In fact, in this case for $\xi < 1$ we have $\rho_{DM} \sim (\mathcal{R}/\xi - 1)\rho_*$ so that DM and stars mass are locally proportional, but for $\xi > 1$, while in non-minimum halo models $\rho_{DM} \sim (\mathcal{R}/\xi - 1)\rho_*$, in the minimum-halo models $\rho_{DM} \sim 2(1 - 1/\xi)\rho_* s \propto r^{-1}$, so that these models are centrally baryon-dominated.

It can be of interest for applications to evaluate the relative amount of dark and visible mass within a prescribed (spatial or projected) radius. The minimum value for this quantity is easily calculated from equations (2) and (13),

$$\frac{M_{DM}(r)}{M_*(r)} \geq \frac{\mathcal{R}_m(\xi)(1+s)}{\xi + s} - 1, \tag{19}$$

where $M_{DM}(r) = M_g(r) - M_*(r)$. In Fig. 1 (middle panel), the mass ratios corresponding to three representative values of r are shown as a function of ξ. For example in the case of a sphere of radius equal to a half-mass radius of the stellar distribution (i.e. $r = r_*$), the minimum value M_{DM}/M_* is less than unity for $\xi > 1$: this is a significant improvement of JJ models with respect to the models of CMZ09, where this ratio cannot be less than unity (see fig. 3 therein).

A similar behaviour is obtained for the ratio of projected DM-to-visible mass within some prescribed aperture R, and from the equation (9) it is easy to show that

$$\frac{M_{pDM}(R)}{M_{p*}(R)} \geq \frac{\mathcal{R}_m(\xi)g(\eta/\xi)}{g(\eta)} - 1. \tag{20}$$

In Fig. 1 (right-hand panel), we plot this quantity as a function of ξ for three representative values of the aperture radius, i.e. $R_e/2$, R_e and $2R_e$. Again the qualitative trend is the same as in the other panels, with minimum value well below unity for $\xi > 1$. Note that for $R = R_e$ and considering the limit of equation (20) for $\xi \to \infty$, we obtain for the mass ratio the value $\simeq 1.43$, in perfect agreement with the analogous result for CMZ09 models.

It is interesting to compare the DM halo profile of JJ models in equation (17) with the NFW profile (Navarro, Frenk & White 1997), that we rewrite for $r < r_t$ (the so-called truncation radius) as

$$\rho_{NFW}(r) = \frac{(\mathcal{R}-1)\rho_n}{f(c)s(\xi_{NFW} + s)^2}, \quad f(c) = \ln(1+c) - \frac{c}{1+c}, \tag{21}$$

where $\xi_{NFW} \equiv r_{NFW}/r_*$ is the NFW scalelength in units of r_*, and $c \equiv r_t/r_{NFW}$: note that in the above equation we impose that the total halo mass M_{DM} is the same as in equation (17). From the asymptotic expansion of ρ_{DM} we already know that ρ_{DM} and ρ_{NFW} at small and large radii cannot, in general, be similar. However, in the case of *minimum halo* with $\xi \geq 1$, near the centre ρ_{DM} increases as $1/r$, so that ρ_{DM} and ρ_{NFW} can be made identical for $r \to 0$ with the additional choice

$$\xi_{NFW} = \sqrt{\frac{\xi}{2f(c)}}. \tag{22}$$

Therefore, once a specific JJ minimum halo model is considered and a radial range fixed, equations (21)–(22) allow us to determine the best-fitting NFW profile with same total mass and central density profile of $\rho_{\rm DM}$ by tuning the value of c. For example, after a simple 'trial-and-error' exploration, we found that over a range extending out to $\simeq 4$–$8R_{\rm e}$, a 'best-fitting' NFW profile can be made to agree with a minimum halo $\rho_{\rm DM}$ with ξ in the range of $\simeq 2$–5, with deviations < 10–20 per cent (at large radii), and < 5 per cent inside $\simeq 4R_{\rm e}$, adopting c in the range of $\approx$10–20, and resulting $r_{\rm NFW}$ in the range of ≈ 0.9–$1.5R_{\rm e}$.

3 THE PHASE-SPACE DF

Having established the *structural* limitations of the models, before solving the Jeans equations, it is useful to discuss some basic property of the phase-space DF of JJ models, in order to exclude *dynamically* inconsistent combinations of parameters (i.e. choices that would correspond to a somewhere negative DF). Fortunately, as discussed extensively in CP92 (see also Ciotti 1996, 1999), it is possible to obtain lower bounds for the OM anisotropy radius as a function of the density slope and the total mass profile, without actually recovering the DF, which is, in general, impossible in terms of elementary functions. More specifically, in CP92 a simple theorem was proved regarding the necessary and sufficient limitations on $r_{\rm a}$ in multicomponent OM models. We also recall that the CP92 result has been shown to be just a very special case of a class of important and more general inequalities connecting the local density slope and the anisotropy profile in consistent spherical models [the so-called Global Density Slope – Anisotropy Inequality (GDSAI), e.g. see de Bruijne et al. 1996; An & Evans 2006; Ciotti & Morganti 2009, 2010a,b; van Hese, Baees & Dejonghe 2011].

Thus, following the standard nomenclature (e.g. Binney & Tremaine 2008), we assume for the stellar component a DF with the OM parametrization:

$$f = f(Q), \quad Q \equiv \mathcal{E} - \frac{J^2}{2r_{\rm a}^2}, \tag{23}$$

where $\mathcal{E} = \Psi_{\rm T} - v^2/2$ and J are the relative energy and angular momentum modulus of each star (per unit mass), respectively, and $\Psi = -\Phi$ is the relative potential; moreover the DF is truncated as $f(Q) = 0$ for $Q < 0$. As a central BH of mass $M_{\rm BH}$ is added at the centre of the galaxy, the total (relative) gravitational potential is $\Psi_{\rm T} = \Psi_{\rm g} + GM_{\rm BH}/r$, and from equation (13)

$$\frac{\Psi_{\rm T}(r)}{\Psi_{\rm n}} \equiv \psi(s) = \frac{\mu}{s} + \frac{\mathcal{R}}{\xi}\ln\frac{\xi+s}{s}, \quad \mu = \frac{M_{\rm BH}}{M_*}. \tag{24}$$

As well known the radial ($\sigma_{\rm r}$) and tangential ($\sigma_{\rm t}$) components of the velocity dispersion tensor in OM models are related as

$$\beta(r) \equiv 1 - \frac{\sigma_{\rm t}^2(r)}{2\sigma_{\rm r}^2(r)} = \frac{r^2}{r^2 + r_{\rm a}^2}, \tag{25}$$

so that the fully isotropic case is obtained for $r_{\rm a} \to \infty$, while for $r_{\rm a} = 0$ the galaxy is supported by pure radial orbits. For finite values of $r_{\rm a}$, the velocity dispersion tensor becomes isotropic for $r \to 0$ (in practice for $r < r_{\rm a}$), and fully radially anisotropic for $r \to \infty$ (in practice for $r > r_{\rm a}$). Introducing the augmented density

$$\varrho(r) \equiv \rho_*(r)\left(1 + \frac{r^2}{r_{\rm a}^2}\right), \tag{26}$$

the phase-space DF of the stellar component can be recovered from the inversion integral

$$f(Q) = \frac{1}{\sqrt{8}\pi^2}\frac{\mathrm{d}}{\mathrm{d}Q}\int_0^Q \frac{\mathrm{d}\varrho}{\mathrm{d}\Psi_{\rm T}}\frac{\mathrm{d}\Psi_{\rm T}}{\sqrt{Q-\Psi_{\rm T}}} = \frac{1}{\sqrt{8}\pi^2}\int_0^Q \frac{\mathrm{d}^2\varrho}{\mathrm{d}\Psi_{\rm T}^2}\frac{d\Psi_{\rm T}}{\sqrt{Q-\Psi_{\rm T}}}; \tag{27}$$

an analogous expression holds for the DF of the isotropic DM halo, obtained by using $\varrho = \rho_{\rm DM}$, and $r_{\rm a} = \infty$ in equation (23).

In the above integral, it is intended that ϱ is expressed in terms of $\Psi_{\rm T}$, and the second identity follows from integration by parts when considering spatially untruncated profiles such those of JJ models. Note that the OM inversion for the CMZ09 model is somewhat different (see equations 19– 28 therein, and relative discussion), because for these latter models Q is not defined in terms of the relative potential (the potential in equation 16 is purely logarithmic and so diverges both $r \to 0$ and $r \to \infty$, making the introduction of the relative potential useless), and $f(Q)$ is *not* truncated as a function of Q.

In Sections 3.1 and 3.2, after a general discussion about the limitations on the $r_{\rm a}$ imposed by the request of phase-space consistency, i.e. $f(Q) \geq 0$ over the accessible phase space, we will see how far we can proceed analytically in the recovery of the DF of JJ models with central BH.

3.1 Necessary and sufficient conditions for consistency

Following CP92 a *necessary condition* for the positivity of the DF of each of the mass components of JJ models (stars or DM) in the total (galaxy plus central BH) potential is that

$$\frac{\mathrm{d}\varrho(r)}{\mathrm{d}r} \leq 0 \quad \text{[NC]}. \tag{28}$$

This condition is independent of the behaviour of the other density components of the system. A *weak sufficient condition* for consistency is obtained by requiring that the derivative inside the last integral in equation (27) be positive. Also this condition can be expressed as a function of radius as

$$\frac{\mathrm{d}}{\mathrm{d}r}\left[\frac{\mathrm{d}\varrho(r)}{\mathrm{d}r}\frac{r^2}{M_{\rm T}(r)}\right] \geq 0, \quad \text{[WSC]}, \tag{29}$$

where the total mass profile is given by

$$M_{\rm T}(r) = M_{\rm g}(r) + M_{\rm BH}, \tag{30}$$

and $M_{\rm g}(r)$ is given in equation (13). Therefore, a model failing equation (28) is certainly inconsistent, while a model obeying equation (29) is certainly consistent. It follows that the true boundary in the parameter space separating consistent and inconsistent models – that, in general, can be only determined by direct inspection of the DF – is 'bracketed' by the NC and WSC limits.

Before embarking in the analysis of JJ models, some preliminary consideration is in order. First, about the effect of the central BH on consistency. From equations (29) and (30), it follows quite easily that *if* (1) the component is consistent for $M_{\rm BH} = 0$, and (2) $\mathrm{d}(r^2\mathrm{d}\varrho/\mathrm{d}r)/\mathrm{d}r \geq 0$, *then* the model with central BH is certainly consistent. Note that point (2) is nothing else than the WSC for the considered density profile interpreted as a tracer in the gravitational field of the central BH itself; we will use this result in the following discussion. A second consideration is about the effect of anisotropy. When dealing with OM anisotropic systems, the investigation of the NC and WSC, and the study of the DF positivity, lead to consider

inequalities of the kind

$$F + \frac{G}{s_a^2} \geq 0, \quad s_a \equiv \frac{r_a}{r_*}, \tag{31}$$

which must hold over the domain $\mathcal{C}$ spanned by the functions' argument. In practice, the functions F and G are functions of r (in the case of the NC and WSC) or functions of Q (in the case of the DF). From inequality (31), it follows that all OM models can be divided in two families. When F is nowhere negative over $\mathcal{C}$ (e.g. in the case of a consistent isotropic DF), consistency in the anisotropic case is obtained for

$$s_a \geq s_a^- \equiv \sqrt{\max\left[0, \sup_{\mathcal{C}}\left(-\frac{G}{F}\right)\right]}. \tag{32}$$

If G is also positive over $\mathcal{C}$, then $s_a = 0$ and the system can be supported by radial orbits only. In the second case, F is positive only over some proper subset $\mathcal{C}_+$ of $\mathcal{C}$, and negative (or zero) over the complementary subset $\mathcal{C}_-$. If $G < 0$ somewhere[1] on $\mathcal{C}_-$, then the condition (31) cannot be satisfied and the model is inconsistent. If $G \geq 0$ on $\mathcal{C}_-$, one must consider not only the lower limit s_a^- in equation (32) evaluated over $\mathcal{C}_+$ but also the condition

$$s_a \leq s_a^+ = \sqrt{\inf_{\mathcal{C}_-}\left(-\frac{G}{F}\right)}, \tag{33}$$

and consistency is possible only if $s_a^- < s_a^+$. Summarizing, if $F \geq 0$ then $s_a \geq s_a^-$ for consistency. If $F \leq 0$ over $\mathcal{C}_-$ and $G \geq 0$ there, then the inequality $s_a^- \leq s_a \leq s_a^+$ must be verified. Finally, if over $\mathcal{C}_-$ the function $G < 0$ somewhere, or $s_a^+ < s_a^-$, then inequality (31) cannot be satisfied and, in case of a DF analysis, the model must be rejected as inconsistent.

The first application of equations (28) and (29) to JJ models concerns the consistency of the DM halo. Following the similar analysis in CMZ09, for simplicity we restrict to the isotropic case, and then equation (28) shows the equivalence of the request of monotonicity of $\rho_{\rm DM}$ (Section 2.2) with the NC for a consistent DM halo. Of course, the restriction to isotropic case is quite arbitrary, as the virialized end states of N-body collapses are invariably characterized by some amount of radial anisotropy (e.g. van Albada 1982; Nipoti, Londrillo & Ciotti 2006), but for the present illustrative purposes, this assumption is fully justified. The WSC for a fully isotropic DM halo is worked out analytically in Appendix A. In particular, when restricting to the case of no central BH ($\mu = 0$) we found, quite surprisingly, that the condition imposed by the WSC to the halo *is nothing else than the limit (18) imposed by positivity and monotonicity*. It remains to discuss the effect of a central BH. Following the argument after equation (30), it is not difficult to show (Appendix A) that the addition of the central BH in case of isotropy *reinforces* consistency, i.e. a DM halo that is consistent in absence of central BH, it is certainly consistent when a BH is added. Taken together, the two results above and those in Section 2.2 show that the isotropic DM halo of JJ models with central BH, once *positivity only* of $\rho_{\rm DM}$ is assured, automatically satisfies the NC and WSC conditions, and so it is supported by a nowhere negative phase-space DF.

We now move to the more interesting case of the NC and WSC for the stellar component of OM anisotropic JJ models. First, we recall

[1] In Ciotti (1999) and Ciotti (2000), it is erroneously stated that the model is inconsistent if $G < 0$ *everywhere* on $\mathcal{C}_-$. All the results presented therein are however correct.

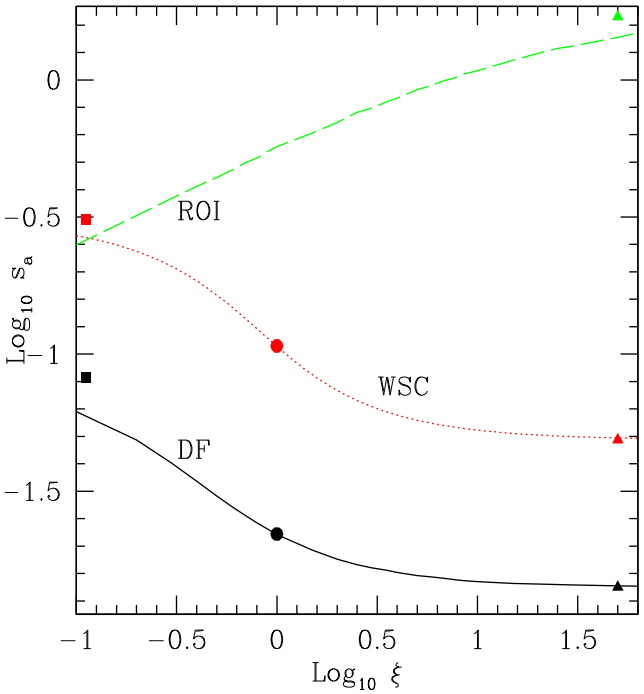

Figure 2. Different limitations on the anisotropy radius $s_a = r_a/r_*$ of the stellar component of JJ models, as a function of $\xi = r_g/r_*$. All the shown results refer to $\mu = 0$, i.e. in absence of the central BH, when the critical values of s_a are rigorously independent of $\mathcal{R}$. The black solid line and the red dotted lines represent the minimum value of s_a obtained directly from the DF and from the WSC, respectively, while the green-dashed curve represents the fiducial lower limit of s_a to prevent the onset of ROI. The triangles show the corresponding values for the CMZ09 model ($s_a \simeq 0.0141$, $s_a \simeq 0.0487$ and $s_a \simeq 1.78$), and the squares for the BH-dominated case ($s_a \simeq 0.082$, see Appendix C; and $s_a \simeq 0.31$, see Appendix A). Finally, the circles correspond to the single component (i.e. $\xi = 1$) Jaffe model ($s_a \simeq 0.02205$, see Appendix C; and $s_a \simeq 0.1068$, see Appendix A).

that NC of Jaffe models just reduces to have $s_a \geq 0$, while from the solution of a cubic equation, the WSC for the one-component Jaffe model gives $s_a \geq s_a^- \simeq 0.1068$ (Ciotti 1999), marked by the red solid circle in Fig. 2. Secondly, in Appendix A, we show that the WSC of the stellar component of JJ models is always in the case described by equation (32), i.e. only s_a^- exists. However, the function at the right-hand side (r.h.s.) of equation (32) in the general case is sufficiently complicated that only a numerical study is feasible. In any case, as in the next section we will determine the *exact* limit on s_a obtained from the DF; here, we just restrict to the case $\mu = 0$. The resulting equation (A8) is much simpler than the general one, and in particular $s_a^- = s_a^-(\xi)$, i.e. when $\mu = 0$ the limit on anisotropy is independent of $\mathcal{R}$ (the dotted red line in Fig. 2). The red triangle at $s_a^- \simeq 0.0487$ marks the position of the WSC limit for the CMZ09 model obtained by solving a cubic equation and that as expected is in accordance with the value of the red line for $\xi \to \infty$. At the opposite limit, we have the BH-dominated case (see Appendix A), with $s_a \simeq 0.31$ marked by the red square, coincident with the value of the red line for $\xi \to 0$, when the total potential becomes that of a central point mass. In practice, from the arguments after equation (30), we have now proved that the stellar component of JJ models with central BH and OM anisotropy is certainly consistent for $s_a > 0.31$, independently of the mass of the central BH and of the DM halo total mass and scalelength. We conclude this introductory analysis by noticing the fact that for JJ

models, the presence of a diffuse halo appears to increase the model ability to sustain radial anisotropy, while for concentrated haloes the consistency of the stellar distribution requires a more isotropic velocity dispersion tensor, as already found in other two-component OM models (Ciotti 1996, 1999; CMZ09).

3.2 Explicit phase-space DF

With the introduction of the dimensionless potential $\psi = \Psi_T/\Psi_n$ and augmented density $\tilde{\varrho} = \varrho/\rho_n$ from equations (24) and (26), respectively, equation (27) writes

$$f(q) = \frac{\rho_n}{\sqrt{8}\pi^2\Psi_n^{3/2}} \int_0^q \frac{\mathrm{d}^2\tilde{\varrho}}{\mathrm{d}\psi^2} \frac{\mathrm{d}\psi}{\sqrt{\psi - q}} = \frac{\rho_n}{\sqrt{8}\pi^2\Psi_n^{3/2}} \left[U(q) + \frac{V(q)}{s_a^2} \right], \tag{34}$$

where $q \equiv Q/\Psi_n$. From equations (23) and (24), it follows that $0 \le q \le \infty$.

In Appendix B, we show that it is possible to invert equation (24) and express analytically the radius as a function of the relative total potential Ψ_T by using the Lambert–Euler W function, obtaining

$$s(\psi) = \frac{\xi}{\frac{\mathcal{R}W}{\mu} - 1}, \quad W = W\left(0, \frac{\mu \mathrm{e}^{\frac{\xi\psi+\mu}{\mathcal{R}}}}{\mathcal{R}}\right), \tag{35}$$

where $W(0, z)$ is one of the two branches of the real determination of the complex function W. In absence of the central BH, we have $\Psi_T = \Psi_g$ and it can be shown that equation (35) reduces to the elementary function

$$s(\psi) = \frac{\xi}{\mathrm{e}^{\psi\xi/\mathcal{R}} - 1}, \tag{36}$$

in agreement with the solution of equation (24) with $\mu = 0$. With the substitution (35) in equation (26), we finally obtain the expression for $\tilde{\varrho}(\psi)$ to be used in equation (27). The derivatives inside the integral are evaluated from the exact relation in equation (B3). We note that the field of application of the W function to physical problems is rapidly expanding (e.g. see Valluri, Jeffrey & Corless 2000; Cranmer 2004; Ciotti & Bertin 2005 for an application to self-consistent toroidal structures, and Veberic 2012; Waters & Proga 2012; Herbst 2015; Ciotti & Pellegrini 2017 for the solution of isothermal accretion on BHs at the centre of galaxies).

In CMZ09, it is shown that for the stellar Jaffe model embedded in a total singular isothermal density profile, and in absence of the central BH, the functions U and V can be expressed as simple linear combinations of exponentials and polylogarithms. Here, not surprisingly, the functions U and V cannot be expressed in terms of known functions, even in absence of the central BH. However, it is interesting to notice that in the case of a dominant central BH (in practice, sufficiently near to the centre), the function $f(q)$ can be expressed by using simple functions (Appendix C).

We now determine numerically the lower limit for consistency of s_a by inspection of the functions U and V. Note that in absence of the central BH ($\mu = 0$), the variable q in equation (34) can be further scaled as $\tilde{q} = q/\mathcal{R}$, while a factor of $\mathcal{R}^{-3/2}$ appears in the functions U and V, as shown in equation (C4). In particular, for these models without BH, the position of the maximum in equation (32) depends on $\tilde{q}$ (and so in terms of q scales linearly with $\mathcal{R}$), but the value of s_a^- is independent of $\mathcal{R}$. The same situation occurs in the CMZ09 models, and in the extreme case of a BH-dominated JJ model, where $\tilde{q} = q/\mu$ (Appendix C, equations C4– C5), and the scaling arguments above apply to the DF with $\mathcal{R}$ replaced by μ. It is numerically found that $U \ge 0$, so that equation (32) applies and only s_a^- exists: the solid line in Fig. 2 shows $s_a^-(\xi)$ determined by the DF in absence of the central BH, for comparison with the other curves presented. Notice how the shape of the critical consistency curve parallels the WSC condition (red dotted line), and how there are consistent models failing the WSC. The black circle at $\xi = 1$ marks the value of the minimum value $s_a \simeq 0.02205$ for the OM one-component Jaffe model (Appendix C). From the figure, it is apparent how the effect of a concentrated DM halo reduces the ability of the stellar component to sustain radial orbits, while the opposite happens for models with $\xi > 1$. As an independent test of the derived DF, the black triangle indicates the limit value of $s_a \simeq 0.0141$ obtained in CMZ09 by numerical inspection of the DF (coincident, as expected, with the limit value of the curve for $\xi \to \infty$), and the black square indicates the value of the BH-dominated case $s_a \simeq 0.082$, coincident with the limit of the curve for $\xi \to 0$.

In Fig. 3, the DF of the stellar component of a selection of representative JJ models is presented in the isotropic (top panel) and anisotropic (bottom panel, $s_a = 0.1$) cases. In both cases, the DFs are shown with and without the effect of the central BH (with $\mu = 10^{-3}$), and for illustration, also the BH-dominated DF (green dashed line) is shown. It is clear how at high (relative) energies the DF of JJ models with central BH is perfectly described by the BH-dominated DF. Also, it is apparent how at high energies the isotropic and anisotropic DFs for models with the same structure are almost identical, a property of OM anisotropy parametrization leading to almost isotropic models in the central regions. It is also important to note how the DFs of models *without* the central BH are higher at high energies than in the analogous models *with* the central BH. Also, notice how models with heavier and more extended haloes and so with higher velocity dispersions at large radii (Fig. 4, top panel) at low relative energies have a lower DF. The physical reason of this behaviour is due to the fact that, qualitatively, the phase-space DF is inversely proportional to the cube of velocity dispersion (because the integral over the velocity space, at fixed position, must reproduce the same value of the local density), so that, empirically, high velocity dispersions corresponds to low values of the DF. This is particularly apparent in the BH-dominated case, with a low DF at high energies and a high DF at low energies. This is also confirmed by the low-energy tail of the DF, which is higher in the anisotropic cases. In fact, from equations (25) and (35), it follows that for $r \to \infty$, the total velocity dispersion profile is proportional to $(\mathcal{A} + s_a^2\mathcal{I})/r^2$, i.e. it is lower for smaller values of s_a. Finally, notice how orbital anisotropy produces a drop of the DF at intermediate energies, with a depression that would be of increasing depth for decreasing values of s_a, finally leading to an inconsistent DF. The curves relative to the anisotropic cases are very similar to the analogous curves in Ciotti & Lanzoni (1997, fig. 2), and C99 (figs 2 and 3) and CMZ09 (fig. 3), revealing the common qualitative behaviour of OM anisotropic DFs near the consistency limit, i.e. the fact that the inconsistency manifests itself, in general, at intermediate energies (see also Ciotti & Morganti 2009 for a discussion).

4 JEANS EQUATIONS WITH OM ANISOTROPY

The Jeans equations for spherical systems with general (radial or tangential) anisotropy has been discussed in Binney & Mamon

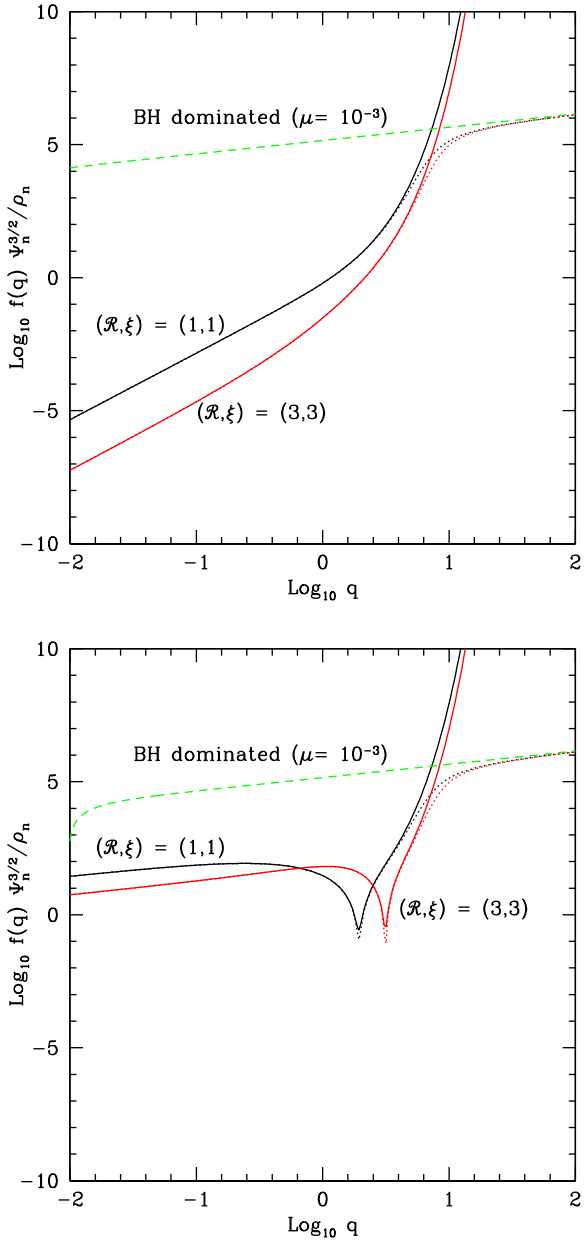

Figure 3. The phase-space DF (normalized to $\rho_n/v_0^3\sqrt{8}\pi^2$) of the stellar component of $\gamma = 1$ (top) and $\gamma = 2$ (bottom) models embedded in a DM halo so that the total density profile is proportional to r^{-2}. Solid lines refer to the case of a fully isotropic stellar component, dotted lines to intermediate values of the (normalized) anisotropy radius s_a (1 for $\gamma = 1$ and 0.1 for $\gamma = 2$), and finally the dashed lines to a value of s_a very near to the critical value for consistency.

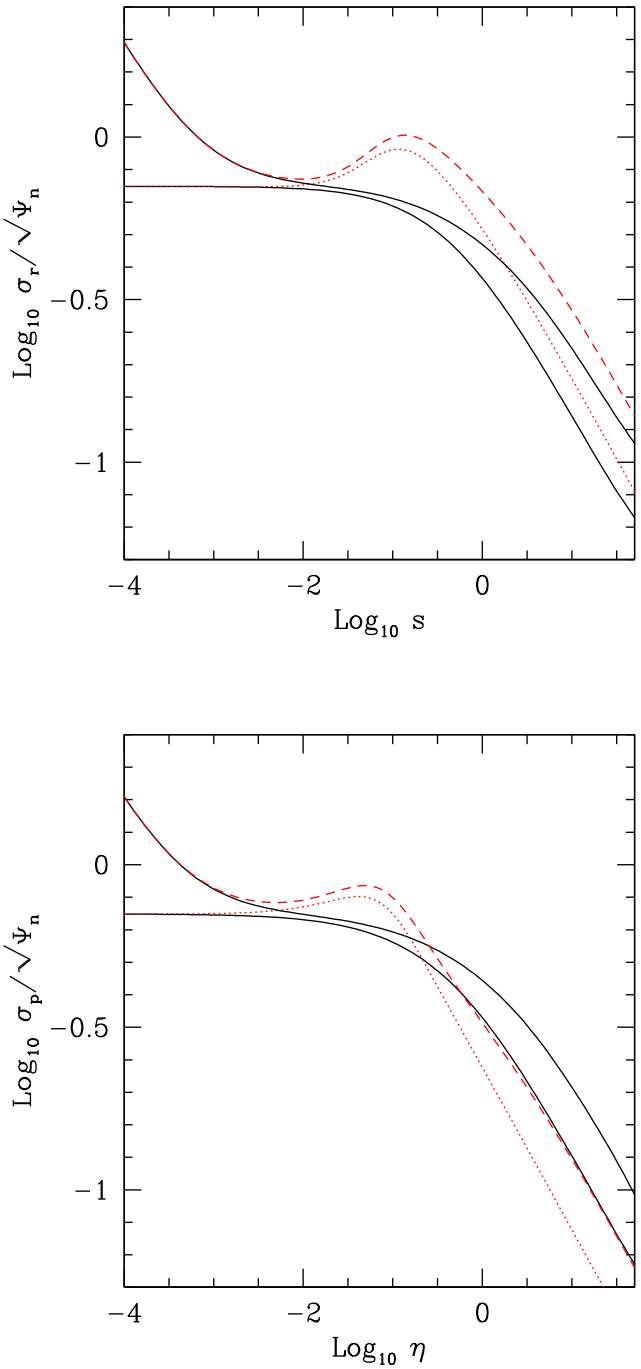

Figure 4. Top panel: radial trend of σ_r of the stellar component of JJ models versus $s = r/r_*$, in some representative case. Black solid lines refer to the isotropic case for the single-component Jaffe model ($\mathcal{R} = 1$, $\xi = 1$, $\mu = 0$), and for a model with central BH and a minimum DM halo ($\mathcal{R} = 3$, $\xi = 3$, $\mu = 10^{-3}$), respectively. Red lines (dotted and dashed) show the profiles for the same models but in a quite anisotropic case, with $s_a = 0.1$. Bottom panel: radial trend of the projected stellar velocity dispersion σ_p versus $\eta = R/r_*$ for the same models in the top panel.

(1982), and in the OM case, the solution can be written as

$$\rho_*(r)\sigma_r^2(r) = \frac{G}{r^2+r_a^2}\int_r^\infty \rho_*(r)M_T(r)\left(1+\frac{r_a^2}{r^2}\right)\mathrm{d}r = \rho_n\Psi_n\frac{\mathcal{A}(s)+s_a^2\mathcal{I}(s)}{s^2+s_a^2}, \quad (37)$$

where $M_T(r)$ is given in equation (30), and the two radial functions

$$\mathcal{I} = \mathcal{R}\,\mathcal{I}_g(s) + \mu\,\mathcal{I}_{BH}(s) \quad \text{and} \quad \mathcal{A} = \mathcal{R}\,\mathcal{A}_g(s) + \mu\,\mathcal{A}_{BH}(s) \quad (38)$$

are the isotropic and purely radial anisotropic components of the velocity dispersion tensor, respectively. In the above formula, the dimensionless mass factors, $\mathcal{R}$ and μ, have been explicitly factorized. For $s_a \to \infty$, we obtain the solution of the fully isotropic case, while for $s_a = 0$, we obtain the purely radial case.

4.1 The velocity dispersion profile

The integration of equation (37) is elementary. In fact, it is formally equivalent to an integration already performed for the different class of two-component Jaffe models in CLR96, where the OM Jeans equation is integrated for a stellar Jaffe distribution, superimposed to Jaffe DM halo of total mass $M_{\rm DM}$, and length scale $r_{\rm DM}$. Therefore, in CLR96, the combined contribution of the stars and of the DM potential to the stellar velocity dispersion profile is given by the sum of two different expressions. Here, instead, only *one* integration is required because the *total* potential is assigned and, in practice, with a suitable renaming of parameters, the formula in CLR96 for the DM halo contribution could be used. However, as we now consider also the effect of the central BH, not included in the models in CLR96 and CMZ09, we give the full set of formulae in homogeneous notation.

For the isotropic component,

$$\mathcal{I}_{\rm g}=\begin{cases}\dfrac{\ln(\xi+s)}{\xi^3(\xi-1)^2}+\dfrac{(3\xi-4)\ln(1+s)}{(\xi-1)^2}-\dfrac{(3\xi^2+2\xi+1)\ln s}{\xi^3}\\ \\ -\dfrac{2s^2(3\xi^2-\xi-1)+s(3\xi+2)(\xi-1)-\xi(\xi-1)}{2\xi^2(\xi-1)s^2(1+s)},\\ \\ -\dfrac{(6s^2+6s-1)(2s+1)}{2s^2(1+s)}-6\ln\dfrac{s}{1+s},\end{cases}\tag{39}$$

where the first expression holds for $\xi\neq 1$, and the second for $\xi=1$. As expected the two expressions agree with equations (A11) and (A5) in CLR96, respectively.[2] The contribution of the BH to the stellar isotropic velocity dispersion profile is given by

$$\mathcal{I}_{\rm BH}=\frac{12s^3+6s^2-2s+1}{3s^3(1+s)}+4\ln\frac{s}{1+s}.\tag{40}$$

Note that this expression could be formally obtained also by considering the limit for $\xi\to 0$ of the function $\mathcal{I}_{\rm g}$, because from equation (2), $\Phi_{\rm J}$ for fixed r and $r_{\rm J}\to 0$ becomes the potential of a point mass.

For the anisotropic part, we have

$$\mathcal{A}_{\rm g}=\begin{cases}\dfrac{\ln(\xi+s)}{\xi(\xi-1)^2}+\dfrac{(\xi-2)\ln(1+s)}{(\xi-1)^2}-\dfrac{\ln s}{\xi}-\dfrac{1}{(1+s)(\xi-1)},\\ \\ -\dfrac{2s+3}{2(1+s)^2}-\ln\dfrac{s}{1+s},\end{cases}\tag{41}$$

where the first expression holds for $\xi\neq 1$ and the second for $\xi=1$, and they agree with equations (A10) and (A4) in CLR96, respectively. The contribution of the central BH to the anisotropic stellar velocity dispersion profile is

$$\mathcal{A}_{\rm BH}=\frac{1+2s}{s(1+s)}+2\ln\frac{s}{1+s},\tag{42}$$

and again it is simple to prove that $At=\mathcal{A}_{\rm BH}$ for $\xi\to 0$. Following equation (15), we also verified equations (39) and (41) considering the limit for $\xi\to\infty$ of the functions $\xi\mathcal{I}_{\rm g}$ and $\xi\mathcal{A}_{\rm g}$, and recovering equations (C2)– (C3) in CMZ09 evaluated for $\gamma=2$.

An insight of the behaviour of $\sigma_{\rm r}$ can be obtained by considering the expansion for $r\to\infty$ and $r\to 0$ of the obtained formulae.

[2] Due to a typo, the sign of the terms inside the square brackets of equation (A11) in CLR96 should be, from left to right, plus, plus, minus, minus.

We begin with the outer galaxy regions. A simple expansion of the functions $\mathcal{A}$ and $\mathcal{I}$ shows that for $r\to\infty$ (in practice, for $r\gg r_*$) the leading order term is the same for the galaxy as for the BH, with

$$\mathcal{I}_{\rm g}\sim\mathcal{I}_{\rm BH}\sim\frac{1}{5s^5}+O(s^{-6}),\tag{43}$$

$$\mathcal{A}_{\rm g}\sim\mathcal{A}_{\rm BH}\sim\frac{1}{3s^3}+O(s^{-4}).\tag{44}$$

The coincidence of the leading term is just due to the fact that for $r\to\infty$ the cumulative mass profile in equation (13) converges to the total galaxy mass, and for the Newton's theorem, this leads to the same contribution to the velocity dispersion as that of a central mass $M_{\rm g}$. Following the same approach adopted in CMZ09, we combine equations (43) and (44), and the leading term of $\sigma_{\rm r}$ in equation (37) for $r\to\infty$ is obtained, for arbitrary value of $r_{\rm a}$, by retaining the leading order term of the expansion of the much simpler expression

$$\rho_*(r)\sigma_{\rm r}^2(r)\sim\rho_{\rm n}\Psi_{\rm n}(\mathcal{R}+\mu)\frac{5s^2+3s_{\rm a}^2}{15s^5(s^2+s_{\rm a}^2)}.\tag{45}$$

In the case of finite $s_{\rm a}$, we have $\sigma_{\rm r}^2\propto 1/(3s)$, while in the fully isotropic case $\sigma_{\rm r}^2\propto 1/(5s)$: as expected, the isotropic $\sigma_{\rm r}$ is lower than in the case of finite $r_{\rm a}$, when the outer regions become populated by radial orbits only. As expected, equation (45) agrees with the analogous expression obtained for the two-component model briefly discussed in section 4.4 of CMZ09 (equation 40 therein, for $\gamma=2$ and for a dominant DM halo). This is at variance with the behaviour of the genuine CMZ09 model, where for $r\to\infty$

$$\rho_*(r)\sigma_{\rm r}^2(r)\sim\rho_{\rm n}v_0^2\frac{2s^2+s_{\rm a}^2}{4s^4(s^2+s_{\rm a}^2)}.\tag{46}$$

Therefore, although the full velocity profile of the CMZ09 model is recovered from the limit procedure in equation (15) applied to equations (39)–(41), the limit procedure applied to equation (45) does *not* converge to the asymptotic expansion of the velocity dispersion profile in CMZ09. This is due to the fact that for $\xi\to\infty$ and $r\to\infty$ the integral (37) is *not uniform* in the variables ξ and r, so that the two limits cannot be, in general, exchanged.

The other important region for observational and theoretical works is the galaxy centre: here, the velocity dispersion profile is dominated by the BH contribution. In fact, at the leading order

$$\mathcal{I}_{\rm g}\sim\frac{1}{2\xi s^2}+O(s^{-1}),\quad \mathcal{A}_{\rm g}\sim-\frac{\ln s}{\xi}+O(1),\tag{47}$$

so that for $r\to 0$ the galaxy contribution to the stellar velocity dispersion profile is given by

$$\rho_*(r)\sigma_{\rm r}^2(r)\sim\frac{\rho_{\rm n}\Psi_{\rm n}\mathcal{R}}{\xi s^2}\begin{cases}\dfrac{1}{2}, & s_{\rm a}>0;\\ \\ -\ln s, & s_{\rm a}=0.\end{cases}\tag{48}$$

In particular, if $r_{\rm a}=0$, the central velocity dispersion diverges as $\sigma_{\rm r}^2\propto-\ln s$, while for all values $r_{\rm a}>0$, the central velocity dispersion converges to a finite value, coincident with that of the isotropic case

$$\sigma_{\rm r}^2(0)=\frac{\Psi_{\rm n}\mathcal{R}}{2\xi}.\tag{49}$$

This is relevant from the modelistic point of view, as it is well known that self-gravitating isotropic γ models present a depression of their velocity dispersion near the centre with $\sigma_{\rm r}(0)=0$, except for the

$\gamma = 0$ and $\gamma = 2$ models (e.g. see Bertin, Ciotti & Del Principe 2002 for a general discussion of this phenomenon; see also Binney & Ossipkov 2001). Notice that the value of the central velocity dispersion, in the minimum halo model with $\xi \geq 1$ is, according to equation (18), *independent* of ξ and *coincident* with that of the purely stellar Jaffe model. This shows the danger of a 'blind' use of $\sigma_r(0)$ as a robust indicator of the actual depth and shape of the galaxy potential well.

For the BH, we obtain

$$\mathcal{I}_{\rm BH} \sim \frac{1}{3s^3} + O(s^{-2}), \quad \mathcal{A}_{\rm BH} \sim \frac{1}{s} + O(\ln s), \tag{50}$$

and the formula analogous to equation (48) is

$$\rho_*(r)\sigma_r^2(r) \sim \frac{\rho_n \Psi_n \mu}{s^3} \begin{cases} \frac{1}{3}, & s_a > 0; \\ 1, & s_a = 0. \end{cases} \tag{51}$$

As expected, σ_r^2 diverges as μ/r for $r \to 0$, and with a factor of 3 of difference between the fully radially anisotropic case, and all the other cases with $s_a > 0$ in agreement with the general property of σ_r in the central regions of γ models with a BH (e.g. see C96, Baes & Dejonghe 2004; Baes et al. 2005). We conclude by noticing that equations (48)–(51) are also in accordance with the analogous quantities for the CMZ09 model (equations C5 and C6) and the two-component models in section 4.4 there (equation 44), and with the results in the spherical (isotropic) limit of one and two-component oblate power-law models with central BH in Ciotti & Bertin (2005, equation C3) and in Riciputi et al. (2005, equation A4), evaluated for $\gamma = 2$.

All the relevant properties of σ_r described in this section are illustrated in Fig. 4 (top panel) by a selection of representative JJ models. In particular, the effects of the central BH, of the DM halo and of orbital anisotropy can be clearly seen near the centre and at large radii.

4.2 Projected velocity dispersion

The projected velocity dispersion profile associated with a general anisotropy function $\beta(r)$ is given by

$$\Sigma_*(R)\sigma_p^2(R) = 2\int_R^\infty \left[1 - \beta(r)\frac{R^2}{r^2}\right] \frac{\rho_*(r)\sigma_r^2(r)\, r}{\sqrt{r^2 - R^2}} {\rm d}r, \tag{52}$$

(e.g. Binney & Tremaine 2008), and in the OM case $\beta(r)$ is given in equation (25).

Unsurprisingly the projection integral cannot be evaluated analytically for JJ models in terms of elementary functions. However, as for the spatial velocity dispersion profile interesting information can be obtained outside the core radius and near the centre. In practice, in the external regions, the stellar and total density profiles can be approximated as a pure power law of slope -4. In this region, the projection integral can be evaluated for generic values of s_a and in analogy with equation (45) the asymptotic trend with radius of the projected profile can be obtained by retaining the leading order term of the expansion of

$$\sigma_p^2(R) \sim \frac{8(\mathcal{R}+\mu)\Psi_n}{15\pi\eta}\left[1 + \frac{\eta^4}{2s_a^2(s_a^2+\eta^2)} - \frac{\eta^4(2s_a^2+\eta^2){\rm archsinh}(s_a/\eta)}{2s_a^3(s_a^2+\eta^2)^{3/2}}\right], \tag{53}$$

where $\eta \equiv R/r_*$. The expression in square parentheses converges to 1 in the isotropic case, and to 1/3 for all finite values of s_a. The analogous formula for the CMZ09 limit models is

$$\sigma_p^2(R) \sim v_0^2 \frac{(s_a^2+\eta^2)^{5/2} - \eta^3(2s_a^2+\eta^2)}{4s_a^2(s_a^2+\eta^2)^{3/2}}, \tag{54}$$

and the same considerations made after equation (46) hold.

The case of the central regions is more complicated. In fact, both the integral (52) and the projected surface density Σ_* (see equation 7) are asymptotically dominated by their integrands for $r \to 0$, so that σ_p^2 can be properly defined only as the limit for $R \to 0$ of the ratio of two diverging quantities. For what concerns the galaxy contribution, a simple calculation shows that for $r_a > 0$

$$\sigma_p(0) = \sigma_r(0), \tag{55}$$

where $\sigma_r(0)$ is given by equation (49), again in agreement with equation (33) in CMZ09 for $\gamma = 2$. For $r_a = 0$, instead the central projected velocity dispersion diverges. Therefore, for the stellar component of JJ models and $r_a > 0$, *the projected central velocity dispersion coincides with the central radial component of the isotropic velocity dispersion*. In presence of the central BH, σ_r is dominated by the BH contribution, and so it is the projected velocity dispersion. With some care, from equations (51) and (52) it can be shown that, from equations (51) and (52) and *independently of the value of* $s_a \geq 0$,

$$\sigma_p^2(R) \sim \frac{2\Psi_n\mu}{3\pi\eta}. \tag{56}$$

All the relevant properties of σ_p expressed by the formulae in this section can be noticed in Fig. 4 (bottom panel), where we show the projected velocity dispersion profiles for the same JJ models in the top panel. In particular, Fig. 4 shows a well-known consequence of the OM parametrization, i.e. the fact that the isotropic σ_r profiles (black lines) in the outer regions are below those in the corresponding radially anisotropic cases (red lines), while the opposite holds for the σ_p profiles, due to projection effects on radial orbits in the outer regions, where the line of sight (l.o.s.) direction is almost perpendicular to the stellar orbits.

We conclude in this section by noticing that CMZ09 (equation 39) briefly commented on the spatial and projected velocity dispersion of a two-component galaxy model made by the superposition of a stellar distribution described by a γ model and a DM halo described by a Jaffe model. Of course, when $\gamma = 2$ this family reduces to JJ models in CLR96: in turns, it is easy to check the perfect correspondence of equations (49) and (55) with equation (42) in CMZ09 by assuming there $\mathcal{R} \to \infty$ and $\beta = \xi$, when the model becomes formally identical (in the limiting case of a DM halo 'infinitely massive') to JJ models (without central BH). The formulae (55) and (56) also agree, as expected, with the projection formulae in the spherical limit of the ellipsoidal models with $\gamma = 2$ in Ciotti & Bertin (2005, equations C1 and C7 therein).

5 VIRIAL, POTENTIAL AND KINETIC ENERGIES

Among the several global quantities that are associated with a stellar system, those entering the VT are certainly the most interesting for many observational and theoretical studies (e.g. Ciotti 2000; Binney & Tremaine 2008). For the stellar component of JJ models, we have

$$2K_* \equiv -W_* = -W_{*g} - W_{*BH}, \tag{57}$$

where $K_* = 2\pi \int_0^\infty \rho_*(\sigma_r^2 + \sigma_t^2) r^2 \mathrm{d}r$ is the total kinetic energy of the stars,

$$W_{*g} = -\int \rho_* < \boldsymbol{x}, \nabla\Phi_g > \mathrm{d}^3\boldsymbol{x} = -4\pi G \int_0^\infty r\rho_*(r) M_g(r) \mathrm{d}r, \tag{58}$$

is the interaction energy of the stars with the gravitational field of the galaxy (stars plus DM), and finally

$$W_{*BH} = -4\pi G M_{BH} \int_0^\infty r\rho_*(r)\mathrm{d}r \tag{59}$$

is the interaction energy of the stars with the central BH. For a Jaffe galaxy, W_{*BH} diverges because the stellar density profile diverges near the origin as r^{-2}; instead, this quantity converges for γ models with $0 \leq \gamma < 2$. Therefore, the VT implies that also the volume integral of $\rho_*\sigma^2_{*BH}$ diverges near the origin for a Jaffe galaxy, as can be seen by direct integration of equation (51).

The contribution of the total galaxy potential to $W_{*g} = W_{**} + W_{*DM}$ (where W_{**} is due to the self-interaction of the stellar distribution, and W_{*DM} to the effect of the DM halo) is finite, with the remarkably simple result

$$W_{*g} = -\Psi_n M_* \mathcal{R} \begin{cases} \dfrac{\xi - 1 - \ln\xi}{(\xi-1)^2}, & \xi \neq 1; \\ \dfrac{1}{2}, & \xi = 1; \end{cases} \tag{60}$$

and taking the limit as in equation (15), $W_{*g} = -GM_*v_0^2$, in accordance with equation 33 in CMZ09. More generally, it can be shown that W_{*g} is a finite quantity for the stellar component of $\gamma\gamma$ models, provided $0 \leq \gamma < 5/2$ (e.g. for two-component Hernquist model, obtained for $\gamma = 1$). It follows that for this class of models it is possible to define the (three-dimensional) galactic virial velocity dispersion as $\sigma_V^2 = -W_{*g}/M_*$: moreover, from equations (49), (55) and (60) the value of σ_V^2 is proportional to the value of the central projected velocity dispersion $\sigma_p^2(0)$, and the proportionality constant is a function of ξ *only*: for $\xi = 1$, $\sigma_V = \sigma_p(0)$. We also notice the interesting behaviour of W_{*g} as a function of ξ in the minimum halo case. While for increasing $\xi \geq 1$ it follows that $\mathcal{R} = \mathcal{R}_m = \xi$ increases correspondingly to arbitrarily large values, the dimensionless coefficient in equation (60) just increases from $1/2$ for $\xi = 1$ to 1 for $\xi \to \infty$, due to the fact that in minimum-halo case, more massive haloes are necessarily more and more extended, with a compensating effect on the depth of the total potential.

As well known, in multicomponent systems, the virial energy W of a given component is *not* the gravitational energy of the component itself in the total potential. For this reason, we now calculate explicitly the different contributions to the potential energy U_* of the stellar component of JJ models, and we also show how to obtain the expression of W_{**} and W_{*DM} in a simple way. As for the interaction energy W_*, also for the potential energy U_*, holds the decomposition

$$U_* = U_{*g} + U_{*BH}, \tag{61}$$

where

$$U_{*g} = U_{**} + U_{*DM} = \frac{1}{2}\int \rho_*\Phi_* \mathrm{d}^3\boldsymbol{x} + \int \rho_*\Phi_{DM}\mathrm{d}^3\boldsymbol{x}, \tag{62}$$

and

$$U_{*BH} = \int \rho_*\Phi_{BH}\mathrm{d}^3\boldsymbol{x} = -4\pi G M_{BH}\int r\rho_*(r)\mathrm{d}r = W_{*BH}. \tag{63}$$

Therefore, U_{*BH} diverges as W_{*BH}. From a well-known result, the self-gravitational energy and the virial self-energy of each density component of a multicomponent system coincide, and in our case from equation (60) with $\mathcal{R} = 1$ and $\xi = 1$,

$$U_{**} = W_{**} = -\frac{\Psi_n M_*}{2}, \tag{64}$$

so that we can compute $W_{*DM} = W_{*g} - W_{**}$ without performing additional integrations. The evaluation of U_{*DM} is slightly more complicated, because in principle it would require to substitute $\Phi_{DM} = \Phi_g - \Phi_*$ in the second integral in equation (60), and therefore compute two integrals. But we adopt a different strategy and compute the integral

$$B_{*g} \equiv \int \rho_*\Phi_g \mathrm{d}^3\boldsymbol{x} = -\Psi_n M_* \mathcal{R} \begin{cases} \dfrac{\ln\xi}{\xi - 1}, & \xi \neq 1; \\ 1, & \xi = 1; \end{cases} \tag{65}$$

so that from equation (60),

$$U_{*DM} = B_{*g} - 2U_{**}, \tag{66}$$

and finally, U_{*g} is obtained by adding U_{**}.

Note that B_{*g} *is not* the gravitational energy U_{*g} of the stars in the galaxy total potential, U_{*g}. Yet, B_{*g} is not just an useful mathematical quantity, but it has an important physical interpretation, and together K_* plays a fundamental role in the theory of galactic winds and X-ray emission of early-type galaxies. In fact, the energy per unit time to be provided to the ISM of early-type galaxies (for example by supernova explosion, thermalization of stellar winds and AGN feedback) required to steadily extract the mass losses of stars, injected over the galaxy body at the rate $\dot{\rho}_{inj} = \alpha(t)\rho_*$ is given by $L_{grav} = \alpha(t)|B_{*g}|$ (e.g. see Pellegrini 2011, 2012; Posacki, Pellegrini & Ciotti 2013). A nice feature of JJ models is that B_{*g} is finite and given by a remarkably simple expression, at variance with the situation of CMZ09 models, where this quantity would diverge, or other two-component models, where B_{*g} is given by quite cumbersome formulae. Therefore, JJ models provide a very simple framework to estimate the energetic of galactic gas flows hosted by X-ray emitting early-type galaxies.

5.1 Stability

Another particularly relevant application of the VT is in the field of model stability, i.e. the determination of the conditions required to prevent the onset of the so-called ROI. In fact, it is well known that stellar systems supported by a large amount of radial orbits are, in general, unstable (e.g. Fridman & Polyachenko 1984, and references therein). A stability analysis is obviously well beyond the task of this work, but we can obtain some quantitative information by investigating the value, as a function of the model parameters, of the stability indicator

$$\Xi \equiv \frac{2K_{*r}}{K_{*t}} = -\frac{4}{2 + W_{*g}/K_{*r}}, \tag{67}$$

where K_{*r} and $K_{*t} = K_* - K_{*r}$ are the total kinetic energies of the stellar component of JJ models, associated with the radial and tangential components of the velocity dispersion tensor, respectively, and the last expression is obtained by evaluating K_{*t} from the VT. Of course, we exclude the effect of the central BH, due to the formal divergence of the kinetic energy K_{*BH} discussed in the previous section. From its definition $\Xi \to 1$ for $s_a \to \infty$ (globally isotropic models), while $\Xi \to \infty$ for $s_a \to 0$ (fully radially anisotropic models).

Numerous investigations of one-component systems have confirmed that the onset of ROI is, in general, prevented by the empirical requirement that $\Xi < 1.7 \pm 0.25$; the exact value of the limit is model dependent (see e.g. Merritt & Aguilar 1985; Bertin & Stiavelli 1989; Saha 1991, 1992; Bertin et al. 1994b; Meza & Zamorano 1997; Nipoti, Londrillo & Ciotti 2002). Here, we are considering two-component systems; however, *N*-body simulations have shown that the presence of a DM halo does not change very much the situation with respect to the one-component systems (e.g. see Stiavelli & Sparke 1991; Nipoti et al. 2002). In our case, we assume as a fiducial maximum value for stability 1.7.

Note that from equation (60) and volume integration of equation (37) with $\mu = 0$, equation (67) shows that Ξ is independent of $\mathcal{R}$. Unfortunately, $K_{*\mathrm{r}}$ cannot be expressed by using elementary functions, so that we explore numerically the fiducial stability condition $\Xi(s_\mathrm{a}, \xi) = 1.7$. In Fig. 2, with green dashed curve we plot the resulting lower bound for stability $s_\mathrm{a}(\xi)$. It is apparent that the critical value of s_a increases with ξ, and this is due to the fact that a spatially extended DM halo increases the contribution to the kinetic energy of the velocity dispersion in the outer parts that, in the OM case, are radially anisotropic. Therefore, in order to guarantee stability in presence of an extended DM halo, the permitted amount of radial orbits must correspondingly reduce, and larger values of s_a are needed. As a limit case the green triangle marks the position of the stability indicator for the limit models in CMZ09, with a limit value of $s_\mathrm{a} \simeq 1.78$. The opposite situation occurs when the DM halo is more concentrated than the stellar component, because in this case the velocity dispersion is increased preferentially in the central regions, that in the OM case are in practice isotropic, and so a larger amount of radial orbits can be supported. All these trends nicely agree with those found for different families of one- and two-component γ models (Ciotti 1996, 1999, see also Carollo et al. 1995). We finally notice how the stability criterion requires minimum anisotropy radii appreciably larger than those obtained from the consistency analysis (see Section 3.2), and so it is likely that the maximally radially anisotropic models with positive DF would be prone to develop ROI.

6 CONCLUSIONS

The family of spherical, two-component galaxy models with the stellar density distribution described by the Jaffe profile, embedded in a DM halo such that the *total* density distribution is also a Jaffe profile, is presented. The DM halo is defined as the difference between the total and the stellar density distributions. A BH is added at the centre of a system, and the dynamics of the stellar component is described by the OM anisotropy profile. The models are fully determined once the total stellar mass (M_*) and scalelength (r_*) are assigned, together with the total-to-stellar mass ratio ($\mathcal{R}$), the total-to-stellar scalelength ratio (ξ), the BH-to-stellar mass ratio (μ) and finally the anisotropy radius (r_a) of the stellar distribution. These models represent a generalization of the CMZ09 models, where the total density profile was fixed at r^{-2} at all radii. In fact JJ models, while retaining interesting properties such as a realistic stellar density profile and a total density profile that can be described as an arbitrarily large radial range by a r^{-2} profile, have a finite total mass and a central BH. At the same time, they still allow for an almost complete analytical treatment, and several quantities of interest in observational and theoretical works have remarkably simple explicit expressions. The main results can be summarized as follows:

(i) After providing a summary of the structural quantities of observational interest for JJ models, for the more general family of two-component $\gamma\gamma$ models, we derive analytically the constraints on $\mathcal{R}$ and ξ needed to assure positivity and monotonicity of the DM halo density distribution. For a given value of ξ, the model corresponding to the minimum value allowed for $\mathcal{R}$ is called *minimum halo model*. In JJ models (in which the positivity and monotonicity limits coincide), $\mathcal{R} \geq \max(\xi, 1/\xi)$. Near the origin the density profile of the DM halo diverges as $\rho_\mathrm{DM} \propto r^{-2}$, but in the minimum halo model with $\xi > 1$ the models are centrally 'baryon dominated', with $\rho_\mathrm{DM} \propto r^{-1}$.

(ii) It is shown that the models presented in CMZ09 are limit cases of JJ models (in absence of the central BH), and we provide the framework to derive all the structural and dynamical quantities of the CMZ09 models from those of JJ models.

(iii) The minimum value of anisotropy radius r_a, corresponding to a dynamically consistent stellar component (i.e. characterized by a nowhere negative DF), is first estimated by using the necessary and sufficient conditions given in CP92. It is shown that in absence of the central BH the minimum value of r_a so determined is a function of ξ only. The critical r_a decreases for increasing ξ, i.e. as already found in other two-component models, a DM halo more extended than the stellar distribution increases the ability of the stellar component to sustain radial anisotropy. On the contrary, more concentrated DM haloes (and in particular a central BH) require a more isotropic orbital distribution. The preliminary consistency analysis is also performed for the DM halo, and it is proved that for isotropic DM haloes in JJ models with $\mu = 0$ the conditions of positivity, monotonicity and phase-space consistency coincide; the addition of a central BH reinforces consistency.

(iv) We then moved to study the phase-space DF for the stellar component as given by OM inversion. We found that for JJ models it is possible to express analytically the dependence of radius on the total potential in terms of the Lambert–Euler *W* function, allowing for a fast and accurate recovery of the DF. In the case of no BH ($\mu = 0$), the resulting expression reduces to elementary functions, and in the limit case of a dominant BH (or a very concentrated DM halo corresponding to $\xi \to 0$), the DF itself can be obtained in terms of elementary functions. After presenting a few representative cases of DFs, corresponding to different choices of $\mathcal{R}$, ξ and r_a, we determined numerically the (minimum) critical value of r_a as a function of the model parameters and found that the obtained curve nicely parallels the bound given by the sufficient condition in CP92. We showed that in absence of the central BH, and in the case of a dominant BH, the critical r_a depends only on ξ, and it is independent of $\mathcal{R}$ and μ, respectively. In general, we confirmed that DM haloes more extended than the stellar component increase the amount of radial anisotropy that can be supported by a positive DF, while the opposite happens in the case of concentrated haloes (or in presence of a central BH), again in accordance with previous findings relative to different two-component OM models. Quite unexpectedly, from the inspection of the analytical DF, and by independent numerical verification, we found that the single-component Jaffe model *cannot* support purely radial orbits in the OM formulation, as detailed in Appendix C.

(v) The Jeans equations for the stellar component are solved explicitly for generic values of the model parameters in terms of elementary functions. The asymptotic expansions of σ_r and σ_p for $r \to 0$ and $r \to \infty$ are obtained, and in particular, it is shown that when $\mu = 0$ and for all values of $r_\mathrm{a} > 0$ (isotropic case included), $\sigma_\mathrm{r}^2(0) = \Psi_\mathrm{n}\mathcal{R}/(2\xi)$. In this case, by asymptotic expansion of the projection integral with $r_\mathrm{a} > 0$, the value of the anisotropy radius, $\sigma_\mathrm{p}(0) = \sigma_\mathrm{r}(0)$, is also shown independently. In presence of the BH,

in the central regions, $\sigma_r^2 \propto r^{-1}$ with a coefficient that is different for $r_a = 0$ or $r_a > 0$. In projection, due to a compensating effect, $\sigma_p^2(R) \sim 2\Psi_n \mu r_*/(3\pi R)$ for $r_a \geq 0$.

(vi) Finally, the analytical expressions of relevant quantities entering the VT, such as the stellar kinetic energy, the virial energy interactions, the potential energies, are derived as a functions of the model parameters. With the aid of the obtained formulae, we determined the minimum value of r_a corresponding to a value of $\simeq 1.7$ of the Friedmann–Poliachenko–Shuckman instability indicator, so that more anisotropic models are prone to the onset of ROI. Again, in line with previous results, the minimum r_a for stability increases for increasing ξ, and in absence of the central BH, its value depends only on ξ, being independent of $\mathcal{R}$.

We conclude by noting that JJ models, albeit highly idealized, suggest a few interesting remarks of observational and theoretical character. For example, after having fixed the properties of the models by using available observational constraints (e.g. see Negri et al. 2014), one could use JJ models to investigate how the so-called *sphere of influence* of the BH depends on the galaxy properties and how its definition is affected by orbital anisotropy. Following a preliminary study (Ziaee Lorzad 2016), it is natural to define the radius of the sphere of influence as the distance from the galaxy centre where the quantity

$$\Delta\sigma^2 \equiv \frac{\sigma_{*g}^2 + \sigma_{*BH}^2 - \sigma_{*g}^2}{\sigma_{*g}^2} = \frac{\mu \mathcal{I}_{BH}(r)}{\mathcal{R}\mathcal{I}_g(r)} \tag{68}$$

reaches some prescribed value (for example 20 per cent, 50 per cent, 100 per cent) as a functional, structural and dynamical properties of the galaxy itself. JJ models could also be used to obtain some preliminary estimate of structural/dynamical properties of high-redshift galaxies (e.g. see section 4.4.1 in Vanzella et al. 2017), thanks to the very simple expressions of their virial quantities.

Another interesting application of JJ models is in the field of BH accretion because, as shown in Ciotti & Pellegrini (2017), it is possible to solve analytically the generalized isothermal Bondi accretion problem in Jaffe (or Hernquist) potentials with a central BH. As the total density profile of JJ models is a Jaffe law, it follows that for these models we can solve *both* the accretion problem for the gas and the Jeans equations for the stellar component. Moreover, JJ models allow for the computation of the stellar kinetic energy, a quantity strictly related to the average temperature of the ISM in early-type galaxies. As the gas temperature determines the location of the Bondi radius, JJ models represent a fully analytical family of self-consistent stellar dynamical-hydrodynamical models, which will allow us to compare the relative position of the sonic radius and the radius of the sphere of influence as a function of the galaxy properties.

ACKNOWLEDGEMENTS

We thank the anonymous referee for useful comments, and John Magorrian and Silvia Pellegrini for interesting discussions on the models. LC thanks G. Bertin, J. Binney, T. de Zeeuw, W. Evans, D. Lynden-Bell, D. Merritt and S. Tremaine for useful comments on Appendix C. AZ acknowledges the Department of Physics and Astronomy of Padua University, where a preliminary study of JJ models has been the subject of her Master Thesis.

REFERENCES

An J. H., Evans N. W., 2006, ApJ, 642, 752
Baes M., Dejonghe H., 2004, MNRAS, 351, 18
Baes M., Dejonghe H., Buyle P., 2005, A&A, 432, 411
Bertin G., 2000, Dynamics of Galaxies. Cambridge Univ. Press, Cambridge
Bertin G., Stiavelli M., 1989, ApJ, 338, 723
Bertin G. et al., 1994a, A&A, 292, 381
Bertin G., Pegoraro F., Rubini F., Vesperini E., 1994b, ApJ, 434, 94
Bertin G., Ciotti L., Del Principe M., 2002, A&A, 386, 149
Binney J., Mamon G., 1982, MNRAS, 200, 361
Binney J., Ossipkov L. P., 2001, in Ossipkov L. P., Nikiforov I. I., eds, Stellar Dynamics: from Classic to Modern, Proceedings of the International Conference. Sobolev Astronomical Institute, Saint Petersburg, p. 317
Binney J., Tremaine S., 2008, Galactic Dynamics, 2nd edn. Princeton Univ. Press, Princeton, NJ
Buyle P., Hunter C., Dejonghe H., 2007, MNRAS, 375, 773
Cappellari M. et al., 2007, MNRAS, 379, 418
Carollo C. M., de Zeeuw P. T., van der Marel R. P., 1995, MNRAS, 276, 1131
Ciotti L., 1996, ApJ, 471, 68
Ciotti L., 1999, ApJ, 520, 574
Ciotti L., 2000, Lecture Notes on Stellar Dynamics (Pisa: Scuola Normale Superiore Ed.)
Ciotti L., Bertin G., 2005, A&A, 437, 419
Ciotti L., Lanzoni B., 1997, A&A, 321, 724
Ciotti L., Morganti L., 2009, MNRAS, 393, 179
Ciotti L., Morganti L., 2010a, MNRAS, 401, 1091
Ciotti L., Morganti L., 2010b, MNRAS, 408, 1070
Ciotti L., Ostriker J. P., 2012, in Kim D.-W., Pellegrini S., eds, AGN Feedback in Elliptical Galaxies: Numerical Simulations, in Hot interstellar Matter in Elliptical Galaxies, ASSL, Vol. 378. Springer, Heidelberg, Dordrecht, London, New York. p. 83
Ciotti L., Pellegrini S., 1992, MNRAS, 255, 561 (CP92)
Ciotti L., Pellegrini S., 2017, ApJ, 848, 29
Ciotti L., Renzini A., 1993, ApJ, 416, L49
Ciotti L., Lanzoni B., Renzini A., 1996, MNRAS, 282, 1 (CLR96)
Ciotti L., Morganti L., de Zeeuw P. T., 2009, MNRAS, 393, 491 (CMZ09)
Corless R. M., Gonnet G. H., Hare D. E. G., Jeffrey D.J., Knuth D.E., 1996, Adv. Comput. Math., 5, 329
Cranmer S. R., 2004, Am. J. Phys, 72, 1397
Czoske O., Barnabe M., Koopmans L. E. V., Treu T., Bolton A. S., 2008, ApJ, 384, 987
de Bruijne, Jos H. J., van der Marel R. P., de Zeeuw P. T., 1996, MNRAS, 282, 909
De Vaucouleurs G., 1948, Ann. d'Astrophys., 11, 247
Dehnen W., 1993, MNRAS, 265, 250
Dye S., Evans N. W., Belokurow V., Warren S. J., Hewett P., 2008, MNRAS, 388, 384
Evans N. W., An J., Bowden A., Williams A. A., 2015, MNRAS, 450, 846
Fridman A. M., Polyachenko V. L., 1984, Physics of Gravitating Systems. Springer, New York
Gavazzi R., Treu T., Rhodes J. D. Koopmans L. V. E., Bolton A. S., Burles S., Massey R. J., Moustakas L. A., 2007, ApJ, 667, 176
Gerhard O., Kronawitter A., Saglia R. P., Bender R., 2001, AJ, 121, 1936
Herbst R. S., 2015, PhD thesis, Univ. Witwatersrand
Hernquist L., 1990, ApJ, 536, 359
Hiotelis N., 1994, A&A, 291, 725
Jaffe W., 1983, MNRAS, 202, 995
Kochanek C. S., 1994, ApJ, 436, 56
Koopmans L. V. E., Treu T., Bolton A. S., Burles S., Moustakas L. A., 2006, ApJ, 649, 599
Kormendy J., Ho L. C., 2013, ARA&A, 51, 511
Magorrian J. et al., 1998, AJ, 115, 2285
Merritt D., 1985a, AJ, 90, 1027
Merritt D., 1985b, MNRAS, 214, 25P
Merritt D., Aguilar L. A., 1985, MNRAS, 217, 787
Meza A., Zamorano N., 1997, AJ, 490, 136
Naab T., Ostriker J. P., 2007, MNRAS, 366, 899
Navarro J. F., Frenk C. S., White S. D. M., 1997, ApJ, 490, 493
Negri A., Posacki S., Pellegrini S., Ciotti L., 2014, MNRAS, 445, 1351
Nipoti C., Londrillo P., Ciotti L., 2002, MNRAS, 332, 901
Nipoti C., Londrillo P., Ciotti L., 2006, MNRAS, 370, 681

Nipoti C., Treu T., Bolton A. S., 2008, MNRAS, 390, 349
Oldham L. J., Evans N. W., 2016, MNRAS, 462, 298
Osipkov L. P., 1979, Pis'ma Astron. Zh., 5, 77
Pellegrini S., 2011, ApJ, 738, 57
Pellegrini S., 2012, in Kim D.-W., Pellegrini S., eds, Hot Gas Flows on Global and Nuclear Galactic Scales, in Hot interstellar Matter in Elliptical Galaxies, ASSL, Vol. 378, p. 21
Poci A., Cappellari M., McDermid R. M., 2017, MNRAS, 467, 1397
Posacki S., Pellegrini S., Ciotti L., 2013, MNRAS, 433, 2259
Richstone D. O., Tremaine S., 1984, ApJ, 286, 27
Riciputi A., Lanzoni B., Bonoli S., Ciotti L., 2005, A&A, 443, 133
Rix H. W., de Zeeuw P. T., Cretton N., van der Marel R. P., Carollo C. M., 1997, ApJ, 488, 702
Rusin D., Kochanek C. S., 2005, ApJ, 623, 666
Rusin D., Kochanek C. S., Keeton C. R., 2003, ApJ, 595, 29
Saha P., 1991, MNRAS, 148, 494
Saha P., 1992, MNRAS, 254, 132
Sersic J. L., 1963, BAAA, 6, 99
Shankar F. et al., 2017, ApJ, 840, 34
Stiavelli M., Sparke L. S., 1991, ApJ, 382, 466
Tremaine S., Richstone D. O., Byun Y.-I., Dressler A., Faber S. M., Grillmair C., Kormendy J., Lauer T. R., 1994, AJ, 107, 634
Treu T., Koopmans L. V. E., 2002, ApJ, 575, 87
Treu T., Koopmans L. V. E., 2004, ApJ, 611, 739
van Albada T. S., 1982, MNRAS, 201, 939
van den Bosch R. C. E., van de Ven G., Verolme E. K., Cappellari M., de Zeeuw P. T., 2008, MNRAS, 385, 647
van Hese E., Baees M., Dejonghe H., 2011 ApJ, 726, 80
Valluri S. R., Jeffrey D. J., Corless R. M., 2000, Can. J. Phys., 78, 823
Vanzella E. et al., 2017, MNRAS, 467, 4304
Veberic D., 2012, Comput. Phys. Commun., 183, 2622
Waters T. R., Proga D., 2012, MNRAS, 426, 2239
Ziaee Lorzad A., 2016, Master thesis (unpublished), Padua Univ.

APPENDIX A: POSITIVITY AND MONOTONICITY OF THE DM HALO IN $\gamma\gamma$ MODELS

The condition for the *positivity* of the DM halo density profile $\rho_{\rm DM}$ in $\gamma\gamma$ models with $0 \leq \gamma < 3$ is established from equation (17) as

$$\mathcal{R} \geq \frac{(\xi + s)^{4-\gamma}}{\xi(1+s)^{4-\gamma}}, \qquad s \geq 0. \tag{A1}$$

Therefore, $\mathcal{R}$ must be greater than or equal to the *maximum* $\mathcal{R}_{\rm m}(\xi, \gamma)$ of the radial function at r.h.s.: note that $\mathcal{R}_{\rm m}$ is the *minimum* value of $\mathcal{R}$ in order to have a nowhere negative DM halo. Simple algebra shows that the maximum is attained at infinity for $\xi < 1$, and at the origin for $\xi > 1$, while for $\xi = 1$ the radial function is identically equal to 1. From equation (A1), it follows that

$$\mathcal{R} \geq \mathcal{R}_{\rm m}(\xi, \gamma) = \max\left(\frac{1}{\xi}, \xi^{3-\gamma}\right), \tag{A2}$$

and for $\gamma = 2$, we obtain equation (18).

The *monotonicity* condition for $\rho_{\rm DM}$ is obtained by requiring that $\mathrm{d}\rho_{\rm DM}/\mathrm{d}r \leq 0$, i.e.

$$\mathcal{R} \geq \frac{(\xi + s)^{5-\gamma}(\gamma + 4s)}{(1+s)^{5-\gamma}\xi(\xi\gamma + 4s)}, \quad s \geq 0. \tag{A3}$$

Again we must determine the maximum $\mathcal{R}_{\rm mon}(\xi, \gamma)$ of the r.h.s. of the equation above. It is easy to show that for $\gamma = 0$

$$\mathcal{R}_{\rm mon}(\xi, 0) = \max\left(\frac{1}{\xi}, \xi^4\right), \tag{A4}$$

while for $0 < \gamma < 1$

$$\mathcal{R}_{\rm mon}(\xi, \gamma) = \max\left(\frac{1}{\xi}, f_+\right), \tag{A5}$$

where f_+ is the value of the r.h.s. of equation (A3) at the critical point

$$s_+(\xi, \gamma) = \frac{\sqrt{\gamma[\gamma\xi^2 + \xi(5-3\gamma) + \gamma]} - \gamma(1+\xi)}{10}: \tag{A6}$$

$f_+ \to \xi^4$ and $f_+ \to \xi^2$ for $\gamma \to 0^+$ and $\gamma \to 1^-$, respectively. Finally, for $1 \leq \gamma < 3$ (and so in particular for JJ models, or for two-component Hernquist models that could be constructed by using the same approach of JJ models), it can be shown, quite surprisingly, that the monotonicity condition coincides with the positivity condition, and so $\mathcal{R}_{\rm mon}$ is given by equation (A2).

The application of the WSC to the isotropic DM halo is obtained from equation (26) with $r_{\rm a} \to \infty$, i.e. $\varrho = \rho_{\rm DM}$. The condition in absence of the central BH ($\mu = 0$) reduces to

$$\mathcal{R} \geq \frac{2(s+\xi)^3[6s^3 + 4(1+2\xi)s^2 + (1+7\xi)s + 2\xi]}{4\xi(1+s)^4(3s^2 + 3\xi s + \xi^2)}, \quad s \geq 0. \tag{A7}$$

For $\xi = 1$, the r.h.s. equals 1 independently of s. For $\xi \neq 1$, the determination of the maximum leads to study a fifth-degree equation. Fortunately, it can be proved by inspection that the resulting expression with $s \geq 0$ is negative for $\xi > 1$ (and thus the maximum of equation A7 is reached at $s = 0$), and positive for $0 < \xi < 1$ (and so the maximum is reached for $s \to \infty$). In the two limits, equation (A7) evaluates to ξ and $1/\xi$, respectively, and so we conclude that the isotropic DM halo of JJ models (in absence of central BH) is certainly consistent when $\mathcal{R}$ satisfies the positivity and monotonicity condition in equation (18). We are now in position to consider the effect of the central BH. A direct analysis would lead to a cumbersome expression, to be explored numerically. However, by using the considerations after equation (30), it is simple to show that the additional term due to the BH is positive, and so it reinforces the WSC when the positivity condition on $\rho_{\rm DM}$ is verified.

The application of the WSC to the OM anisotropic stellar component of JJ models leads to the study of a seventh-degree equation and shows that we are in the conditions pertinent to equation (32). In absence of the central BH the dependence on $\mathcal{R}$ disappears,

$$s_{\rm a}^2 \geq -\frac{s^3[s^2 + 2(\xi-1)s - \xi]}{6s^3 + 4(1+2\xi)s^2 + (1+7\xi)s + 2\xi}, \quad s \geq 0, \tag{A8}$$

and we should solve a fifth-degree equation when searching for the maximum of the r.h.s. In Section 3.1, we present the results obtained by numerical inspection of equation above. Restricting further to the case $\xi = 1$ (i.e. reducing to the one-component Jaffe model), the equation to be solved becomes cubic, with $s_{\rm a}^- \simeq 0.1068$ (Ciotti 1999). Finally, the case obtained for $\xi \to 0$ is formally coincident with the case of a dominant central BH (i.e. only $M_{\rm BH}$ is retained in equations 29– 30), and for this limiting case the WSC reduces again to a cubic equation, with solution $s_{\rm a}^- \simeq 0.31$.

APPENDIX B: THE LAMBERT–EULER W FUNCTION

As discussed in Section 3, for JJ models with central BH it is possible to invert equation (24) and express the radius r in terms of the relative total potential by using the Lambert–Euler W function. The integrand in the inversion integral (34) is then obtained in explicit and easily tractable form, without resorting to complicate

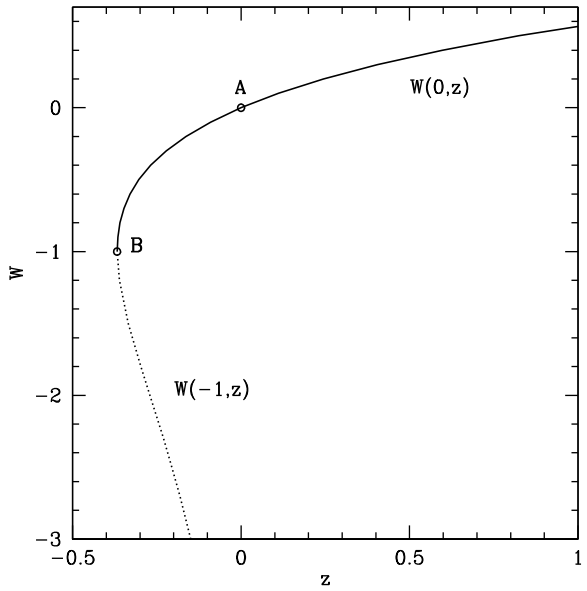

Figure B1. The two branches of the real determination of the Lambert–Euler W function for real argument. The coordinates of the two marked points are $A = (0, 0)$ and $B = (-1/\mathrm{e}, -1)$. The solid line represents the branch $W(0, z)$, and only points at right if point A, with $z \geq 0$, are needed in the inversion formula (35). The dotted line is the $W(-1, z)$ branch.

numerical procedures, because the W function is now fully implemented in the most used computer algebra systems. The function $W(z)$ (see e.g. Corless et al. 1996) is a multivalued complex function defined implicitly by the identity

$$W\mathrm{e}^{W} = z, \tag{B1}$$

and the two real branches $W(0, z)$ and $W(-1, z)$ for real values of z are shown in Fig. B1.

With the transformation of variables $W = (1 + \xi/s)\,\mu/\mathcal{R}$, equation (24) can be rewritten as

$$W + \ln W = \frac{\xi\psi + \mu}{\mathcal{R}} + \ln\frac{\mu}{\mathcal{R}}, \tag{B2}$$

so that equation (35) is obtained by exponentiation of equation (B2) and comparison with equation (B1). It is immediate to conclude that for the present problem the relevant branch is given by $W(0, z)$, restricting to points beyond point A. In fact, when $\psi \to \infty$, the argument in equation (B2) is infinite, $W(0, z) \to \infty$, and from equation (35) $s \to 0$. Instead, when $\psi \to 0$, the argument tends to $\mu/\mathcal{R}\mathrm{e}^{\mu/\mathcal{R}}$, $W \to \mu/\mathcal{R}$, and so from equation (35) $s \to \infty$ from equation (35), as it should.[3] Finally, note that the derivatives inside the integral (34) can be expressed analytically in terms of W itself, because from equation (B1) it follows that

$$\frac{\mathrm{d}W}{\mathrm{d}z} = \frac{W}{z(1+W)}. \tag{B3}$$

APPENDIX C: DF OF OM JAFFE MODEL WITH DOMINANT CENTRAL BH

We report the explicit phase-space DF of a Jaffe model with OM anisotropy and with dominant central BH (i.e. the gravitational field is produced by the BH only, and the stellar distribution is only a tracer). The resulting expression can be interpreted as the asymptotic limit of the DF at high relative energies, i.e. for galactic regions sufficiently near the central BH. By using the nomenclature in equation (34), it is easy to show that the functions U and V can be written as

$$U(q) = \frac{U(\tilde{q})}{\mu^{3/2}}, \quad V(q) = \frac{V(\tilde{q})}{\mu^{3/2}}, \quad \tilde{q} \equiv \frac{q}{\mu}, \tag{C1}$$

where

$$U(\tilde{q}) = \frac{(16\tilde{q}^3 + 40\tilde{q}^2 + 18\tilde{q} + 9)\sqrt{\tilde{q}}}{4(1+q)^3} - \frac{3(3+8\tilde{q})\mathrm{arcsenh}\sqrt{\tilde{q}}}{4(1+\tilde{q})^{7/2}}, \tag{C2}$$

and

$$V(\tilde{q}) = \frac{(13-2\tilde{q})\sqrt{\tilde{q}}}{4(1+\tilde{q})^3} + \frac{3(1-4\tilde{q})\mathrm{arcsenh}\sqrt{\tilde{q}}}{4(1+\tilde{q})^{7/2}}. \tag{C3}$$

The function U is nowhere negative in the range $0 \leq \tilde{q} < \infty$, so the BH-dominated Jaffe models are always in the first case discussed in Section 3.1, and only s_{a}^{-} exists: a numerical evaluation shows that $s_{\mathrm{a}}^{-} \simeq 0.082$, in agreement with the trend of the solid line in Fig. 2 for $\xi \to 0$, when the DM halo 'collapses' to a central point mass.

For completeness, we also report the explicit DF for the stellar component of JJ models with $\xi = 1$ and in absence of the central BH, when the resulting expression reduces to the one-component DF in the OM case. From equation (34), we now have

$$U(q) = \frac{U(\tilde{q})}{\mathcal{R}^{3/2}}, \quad V(q) = \frac{V(\tilde{q})}{\mathcal{R}^{3/2}}, \quad \tilde{q} \equiv \frac{q}{\mathcal{R}}, \tag{C4}$$

with $0 \leq \tilde{q} < \infty$ and

$$\frac{U(\tilde{q})}{4\sqrt{2}} = F_+(\sqrt{2\tilde{q}}) + F_-(\sqrt{2\tilde{q}}) - \sqrt{2}\left[F_+(\sqrt{\tilde{q}}) + F_-(\sqrt{\tilde{q}})\right], \tag{C5}$$

$$\frac{V(\tilde{q})}{4\sqrt{2}} = F_+(\sqrt{2\tilde{q}}) - \frac{F_+(\sqrt{\tilde{q}})}{\sqrt{2}}, \tag{C6}$$

where $F_+(x) = \mathrm{e}^{-x^2}\int_0^x \mathrm{e}^{t^2}\mathrm{d}t$ is the Dawson's function, and $F_-(x) = \mathrm{e}^{x^2}\int_0^x \mathrm{e}^{-t^2}\mathrm{d}t = \sqrt{\pi}e^{x^2}\mathrm{Erf}(x)/2$. The functions above, when combined according to equation (34), are in perfect agreement with those given by Merritt (1985b, equation 6) and Binney & Tremaine (2008). The function U in equation (C5) is positive for alla values of $\tilde{q}$, as shown by the WSC, but the function V in equation (C6) becomes negative for admissible values of $\tilde{q}$, so that r_{a} cannot be arbitrarily small. Numerical evaluation of equation (32) shows that for consistency $s_{\mathrm{a}} \geq s_{\mathrm{a}}^{-} \simeq 0.02205$, in perfect agreement with the solid line in Fig. 2 (obtained from the general DF) for $\xi = 1$.

From this result, one could conclude that the purely radial model does not exist. However, the situation is not so simple. In fact, the DF of a purely radial model can be written in all generality as $f = \delta(J^2)h(\mathcal{E})$, so that for a finite mass, spatially untruncated model

$$\rho(\Psi_{\mathrm{T}}) = \frac{2\pi}{r^2}\int_0^{\Psi_{\mathrm{T}}} \frac{h(\mathcal{E})\mathrm{d}\mathcal{E}}{\sqrt{\Psi_{\mathrm{T}} - \mathcal{E}}}, \tag{C7}$$

(e.g. Ciotti 2000), and the inversion formula can be immediately found (e.g. see Richstone & Tremaine 1984; Oldham &

[3] By definition of W, it follows that $W(y\mathrm{e}^{y}) = y$.

Evans 2016)

$$h(\mathcal{E}) = \frac{1}{\sqrt{2}\pi^2}\frac{\mathrm{d}}{\mathrm{d}\mathcal{E}}\int_0^{\mathcal{E}}\frac{\varrho\,\mathrm{d}\Psi_\mathrm{T}}{\sqrt{\mathcal{E}-\Psi_\mathrm{T}}} = \frac{1}{\sqrt{2}\pi^2}\int_0^{\mathcal{E}}\frac{\mathrm{d}\varrho}{\mathrm{d}\Psi_\mathrm{T}}\frac{\mathrm{d}\Psi_\mathrm{T}}{\sqrt{\mathcal{Q}-\Psi_\mathrm{T}}}, \tag{C8}$$

where $\varrho = r^2\rho$ is expressed in terms of Ψ_T, and the second identity follows from integration by parts when considering spatially untruncated profiles such those of JJ models. As shown by Merritt (1985b, equation 8) and Evans et al. (2015, equation 31), for the purely radial one-component Jaffe model

$$h(\tilde{\mathcal{E}}) = \frac{2\rho_\mathrm{n} r_*^2}{\pi^2\sqrt{\Psi_\mathrm{n}}}\left[\sqrt{2}F_+(\sqrt{\tilde{\mathcal{E}}}) - F_+(\sqrt{2\tilde{\mathcal{E}}})\right], \tag{C9}$$

where $\tilde{\mathcal{E}} \equiv \mathcal{E}/\Psi_\mathrm{n}$. The function is positive at *all* energies, thus showing that the purely radial Jaffe model *is* consistent.

These two seemingly contradictory results indicate that the purely radial case, at least for the Jaffe model, is a singular limit for the OM parametrization. In practice, we have shown that the non-existence of the OM (or others) highly radial models cannot by itself exclude the phase-space consistency of the purely radial configuration. In fact, the following argument, built by using the CP92 approach to the purely radial case, reinforces this conclusion. From the second of equation (C8) it follows immediately that a *sufficient* condition for consistency of the purely radial model is that the derivative inside the integral be non-negative, i.e. in terms of radius

$$\frac{\mathrm{d}\varrho(r)}{\mathrm{d}r} \leq 0, \quad \varrho(r) = r^2\rho(r). \tag{C10}$$

Therefore, in the purely radial model a density profile declining as r^{-2} or faster at all radii is a *sufficient* condition for consistency (in agreement with the result obtained for the Jaffe model), while the OM condition (28) (the analogous of equation (C10) in the limit of vanishing anisotropy radius) is only *necessary* for phase-space consistency. The mathematical reason of the different behaviour is due to the fact that in equation (C7), at variance with the corresponding expression in the OM case, the preparatory derivative of the augmented density is not required to perform the Abel inversion.

This paper has been typeset from a TEX/LATEX file prepared by the author.